附件一

行政院國家科學委員會補助專題研究計畫 ■ 成 果 報 告 □期中進度報告

（計畫名稱）

非包爾-歐本海默分子動力學理論與在光化學中的應用

計畫類別：■個別型計畫　□整合型計畫
計畫編號：NSC 97－2113－M－009－010－MY3
執行期間：：2008 年 8 月 1 日至 2011 年 7 月 31 日

執行機構及系所：國立交通大學應用化學系

計畫主持人：朱超原
共同主持人：
計畫參與人員：碩士級-專任助理人員：蔡琇雅
碩士級-專任助理人員：陳美婷
碩士班研究生-兼任助理人員：張哲源, 黃琮偉, 孔令鈞
博士後研究：李清旭, 雷依波

成果報告類型(依經費核定清單規定繳交)：□精簡報告　■完整報告

本計畫除繳交成果報告外，另須繳交以下出國心得報告：
■出席國際學術會議心得報告

處理方式：除列管計畫及下列情形者外，得立即公開查詢
□涉及專利或其他智慧財產權，□一年□二年後可公開查詢

中　華　民　國　101　年　3 月　24　日

1. “Anharmonic Franck-Condon simulation of the absorption and fluorescence spectra for the low-lying S1 and S2 excited states of pyrimidine,”
L.Yang, **C. Zhu***, J. G.. Yu, and S. H. Lin
Publish on Chem. Phys. (in press, 2012).

Abstract

Intensities and profiles of vibronic spectra of the low-lying singlet excited states were investigated with anharmonic and harmonic Franck-Condon simulations for pyrimidine. The first-order anharmonic correction shows dynamic shift of spectra that is exactly same as difference of reorganization energy between ground and excited states. The first-order correction shows intensity enhancement of absorption and intensity weakening of fluorescence for S_1 state, and dynamic shift is also significant. On the other hand, the first-order correction is negligible for S_2 state. The main spectral progressions are well described by totally symmetry modes ν_{6a}, ν_1 and ν_{12}. One mode from non-total symmetry ν_{16a} contributes to the weak band at $16a^2$ transition for S_1 state. Four ab initio methods were employed in simulation; CASSCF, CASPT2, DFT and TD-DFT, and coupled-cluster singles-doubles (CCSD) and the equation-of-motion (EOM-CCSD) methods. They all work well, but CASSCF method shows the best agreement with experiment for the weak-band intensities.

Introduction

Pyrimidine (1,3-diazine), $C_4H_4N_2$, belongs to the group of diazine ring molecules, whose skeletons serve as building blocks in nature, that may be used as a chemical or molecular model for the single nucleosides (thymine, cytosine and uracil) in nucleic acids . The electronic spectroscopy of the azabenzenes (pyridine, pyrazine and pyrimidine) has been very interesting subject due to its rich excited-state dynamical and photochemical properties, as well as its importance for biologically relevant spectroscopic processes. A variety of computational simulations have been carried out for the S_1 and S_2 absorption and the fluorescence spectra of pyridine and pyrazine. In the present study, we first calculate the equilibrium geometries, vibrational frequencies, vertical and adiabatic excitation energies of the ground state $S_0(^1A_1)$ and the low-lying $S_1(^1B_1)$ and $S_2(^1B_2)$ excited states using CASSCF, CASPT2, CCSD/EOM-CCSD, and DFT/TD-DFT methods. It should be noted that the variational principle in ab. initio quantum chemistry methods can insure better accuracy for excitation energies with higher level method but it does not guarantee better accuracy for equilibrium geometries. Intensities and profiles of vibronic spectra in terms of the Franck-Condon overlapping integrals are most sensitive to geometry difference between excited and ground states. Therefore, the CASSCF method can provide accurate vibronic spectra since it treats electronic ground and excited states in an equal footing and it is especially good for geometry optimization of aromatic molecules in which resonance structures are essential. Then, we simulate the absorption and fluorescence spectra for $S_1(^1B_1)$ state and the absorption spectrum for $S_2(^1B_2)$ state by employing the displaced harmonic oscillator approximation including the first-order anharmonic effect. Furthermore, we analyze the distorted effect that takes into account contribution from non-totally symmetry normal modes and it can be considered as diagonal-part correction of Duschinsky mode-mixing matrix. With analytical formulation of absorption and fluorescence coefficients [35], we can explicitly demonstrate how anharmonic effect influences the shifts of spectral peaks,

relative intensities and profiles of spectra with respect to harmonic Franck-Condon simulation.

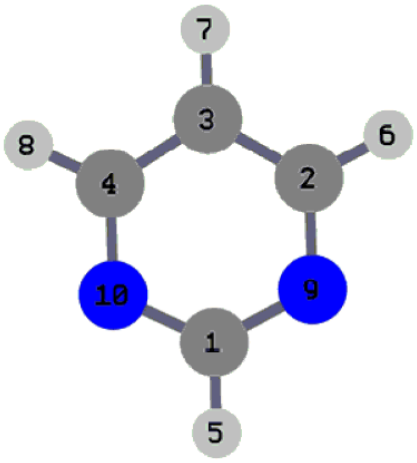

Figure 1. Atom numbering for pyrimidine.

Ab initio methods and anharmonic Franck-Condon factor

We start with perturbation expansion of the *j*th vibrational normal-mode potential energy as

$$V_j(Q) = a_{j2}Q_j^2 + \lambda a_{j3}Q_j^3 + \lambda^2 a_{j4}Q_j^4 + \cdots \tag{1}$$

in which λ is chosen as a perturbation parameter and Q_j is mass-weighted normal-mode coordinate. The first-order correction in perturbation is zero for energy, but is nonzero for wave function with which absorption coefficient is analytically derived as,

$$\alpha(\omega) = \frac{2\pi\omega}{3\hbar}\left|\vec{\mu}_{ba}\right|^2 \int_{-\infty}^{\infty} dt\, e^{it(\omega_{ba}+\Omega_0-\omega)-\gamma_{ba}|t|} \times \exp\left[-\sum_j S_j(1+3\eta_j)\left\{2\bar{\upsilon}_j + 1 - (\bar{\upsilon}_j+1)e^{it\omega_j} - \bar{\upsilon}_j e^{-it\omega_j}\right\}\right] \tag{2}$$

for excitation from electronic ground state *a* to excited state *b* that means $\omega_{ba} > 0$ in eq 2 for adiabatic energy gap between *b* and *a*. Fluorescence coefficient is analytically derived as well

$$I(\omega) = \frac{2\pi\omega}{3\hbar}\left|\vec{\mu}_{ba}\right|^2 \int_{-\infty}^{\infty} dt\, e^{-it(|\omega_{ba}|+\Omega_0-\omega)-\gamma_{ba}|t|} \times \exp\left[-\sum_j S_j(1-3\eta_j)\left\{2\bar{\upsilon}_j + 1 - (\bar{\upsilon}_j+1)e^{it\omega_j} - \bar{\upsilon}_j e^{-it\omega_j}\right\}\right] \tag{3}$$

for excitation from electronic excited state *a* to ground state *b* that means $\omega_{ba} < 0$ in eq 3 for adiabatic energy gap between *b* and *a*. Other quantities are same for both eqs 2 and 3, where $\bar{\nu}_j = (e^{\hbar\omega_j/k_BT} - 1)^{-1}$ is the average phonon distribution, γ_{ba} represents the dephasing constant (with relation to the lifetime $\tau_{ba}=1/\gamma_{ba}$) between two electronic states, and $\vec{\mu}_{ba}$ is the electronic transition dipole moment. The most important quantities Ω_0 and η_j stand for the first-order anharmonic correction given by

$$\Omega_0 = -2\sum_j \eta_j S_j \omega_j \tag{4}$$

and

$$\eta_j = \frac{a_{j3} d_j}{a_{j2}} = \frac{a_{j3} d_j}{0.5\omega_j^2} \tag{5}$$

where ω_j is harmonic vabrational normal-mode frequency, and the Huang-Rhys factor S_j, the displacement d_j, the second coefficient a_{j2} and the third coefficient a_{j3} of potential energy in eq (1) are defined as

$$S_j = \frac{1}{2\hbar}\omega_j d_j^2, \tag{6}$$

$$d_j = Q'_j - Q_j = \sum_n L_{jn}\left(q'_n - q_n\right), \tag{7}$$

$$a_{j2} = \frac{1}{2}\frac{\partial^2 V}{\partial Q_j} = \frac{1}{2}\omega_j^2, \tag{8}$$

and

$$a_{j3} = \frac{1}{3!}\frac{\partial^3 V}{\partial Q_j^3} = \frac{1}{3}K_{j3}. \tag{9}$$

Inserting eq. (9) into eq. (5) leads to

$$\eta_j = \frac{2K_{j3} d_j}{3\omega_j^2} = \frac{K_{j3} d_j^3}{3S_j \hbar\omega_j}. \tag{10}$$

The q'_n and q_n in eq (7) are the mass-weighted Cartesian coordinates at the equilibrium geometries of the electronic excited and ground states, respectively. Transformation matrix **L** in eq (7) can be computed with frequency calculation in G03 and G09 programs. If the dimensionless first-order anharmonic parameter η_j is equal to zero, the absorption and fluorescence coefficients in eqs (2) and (3) are exactly same as those in displaced harmonic oscillator approximation. An anharmonic parameter η_j in eq (10) is expressed in terms of the diagonal element K_{j3} of cubic force constant estimated from G03 and G09 programs. The displacement d_j in eq. (7) that is sensitive to geometry differences between two electronic states is essentially parameter to determine intensities and profile of vibronic spectra. The effective Huang-Rhys factors in Franck-Condon factors are no longer the same from the first-order anharmonic correction; $S'_j = \left(1 \pm 3\eta_j\right)S_j$ (+ for absorption in eq (2) and - for fluorescence emission in eq (3)). Immediate consequence is that mirror image between absorption and fluorescence spectra is broken down accompanying with intensity enhancement of absorption against weakening of fluorescence (or vice versa). At the same time, the harmonic 0→0 excitation energy is shifted by Ω_0 and this can be interpreted as a dynamic correction to spectral position. However, the first-order correction influences little change of band shape in vibronic spectra and for detailed band-shape change the second-order correction is necessary along with the effect like Duschinsky mode-mixing. The first-order anharmonic correction can affect the reorganization energy of ground state $\left(\lambda_0 = E_0^{'} - E_0\right)$ and excited

state $\left(\lambda_{\mathrm{ex}} = E_{ex}^{'} - E_{ex}\right)$ as shown in Fig.2. In comparison with ground-state potential energy defined in eq (1), excited-state potential energy is defined as the left-handed shift with respect to ground state

$$V_{ex-j}\left(Q_j^{'}\right) = a_{j2}(Q_j + d_j)^2 + \lambda a_{j3}(Q_j + d_j)^3 + \lambda^2 a_{j4}(Q_j + d_j)^4 + \cdots \tag{11}$$

for derivation of absorption and fluorescence coefficient in eqs (2) and (3). By adding each-mode contribution to reorganization energy together, we derive expression of reorganization energy within the first-order anharmonic correction as

$$\lambda_0 = \sum_{\mathrm{j}} S_j \hbar\omega_j \left(1 - \eta_j\right) \tag{12}$$

and

$$\lambda_{\mathrm{ex}} = \sum_{\mathrm{j}} S_j \hbar\omega_j \left(1 + \eta_j\right) \tag{13}$$

from which we can immediately find that the reorganization energy differences between the excited state and the ground state is exactly equal to the dynamic shift $\Omega_0 = \lambda_0 - \lambda_{\mathrm{ex}}$ in eq (4), and this is zero within harmonic case.

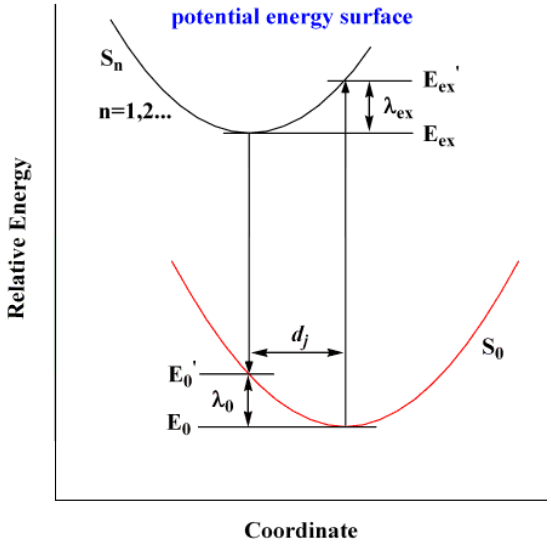

Figure 2. The ground and excited states reorganization energy from the potential energy surfaces, $\lambda_0 = E_0^{'} - E_0$ and $\lambda_{ex} = E_{ex}^{'} - E_{ex}$.

Results and discussion

The present MP2 frequencies are actually utilized in the simulation of both absorption and fluorescence spectra for the two excited states within displaced harmonic and anharmonic oscillator approximations for CASSCF and EOM-CCSD methods, while the B3LYP frequencies is adopted for the TD-B3LYP method. The dephasing constants γ_{ba} in eqs (2) and (3) are chosen as 10 cm^{-1} and 700 cm^{-1} for the excited states $S_1(^1B_1)$ and $S_2(^1B_2)$, respectively. Temperature is taken as 298 K in the simulation as the experimental spectra were measured at room temperature. The intensity of simulated absorption and fluorescence spectra is in the same

unit for S_1 state as shown in Fig.3.

Figure 3 shows that the main progressions of vibronic bands for the S_1 absorption and fluorescence spectra that are well described by mode ν_{6a} accompanied with modes ν_1 and ν_{12}. In fact, this can be easily understood from that the Huang-Rhys factors for the modes ν_{6a}, ν_1, and ν_{12} are 1.566, 0.299, and 0.454, respectively. The overall agreement between experiment and the presently simulated spectra is generally good. However, the highest peak is assigned as the 0-0 vibronic transition for the absorption and the $6a_0^1$ transition for fluorescence spectra from experimental, while the $6a_0^1$ is the strongest transition for both the absorption and fluorescence spectra from the present harmonic calculation. When the anharmonic quantity η_{6a}=-0.004 is included and this makes effective the Huang-Rhys factor for absorption as $S'_{6a}=S_{6a}(1 + 3\eta_{6a}) = 1.547$ and for fluorescence as $S'_{6a}=S_{6a}(1 - 3\eta_{6a}) = 1.585$, the ν_{6a} transition profiles and relative intensity changes in the right direction as illustrated in Figs. 3b and 3b'. Figures 3e and 3e' show that the peak position of the 0-0 excitation from harmonic oscillator approximation has a big discrepancy with experiment observation for both absorption and fluorescence spectra although the best static excitation energy $|\omega_{ab}| = 3.75$ eV is chosen for simulation of the S_1 state. When anharmonic corrections are included in the simulation, Figs. 3b and 3b' show that the peak position of the 0-0 excitation has blue shift Ω_0= 827 cm^{-1} with respect to harmonic oscillator approximation and this leads to a very good agreement with experimental observation. Actually, this dynamic shift was obtained with scaling factor 0.8745 to all anharmonic constants η_j. This kind scaling is widely employed for vibrational frequencies and we think that it is in the same reason to scaling anharmonic constants. We conclude that the first-order anharmonic correction makes spectral peak positions shift and intensities change in the right direction simultaneously for absorption and fluorescence spectra of S_1 state; enhanced intensity of the absorption spectra and weakened intensity of the fluorescence. Finally, we have included the distorted effect for the non-total symmetric mode $16a^2$ as is shown in Figs. 3b, 3e, 3b' and 3e' for a very weak band, which agrees very well with Knight's experimental results. Furthermore, the present EOM-CCSD and TD-B3LYP spectral simulations with anharmonic corrections are similar to the CASSCF simulation, except the highest peak for both absorption and fluorescence of S_1 state now is 0-0 vibronic transition, but the intensity of the weak band is much weaker than that of CASSCF and experiment. We can see that the simulated fluorescence spectrum of S_1 state show better agreement with the experimental results than the simulated absorption spectrum. The discrepancy may be because that the strong experimental absorption spectrum of S_2 state affects the absorption spectrum of S_1 state, while the weak fluorescence spectrum of S_2 state has little effects to the strong fluorescence spectrum of S_1 state during the experiment.

The largest Huang-Rhys factor for the $S_2(^1B_2)$ state is 1.402 for vibrational mode ν_1 accompanied by the other two; 0.044 for the mode ν_{6a} and 0.153 for mode ν_{12}. Figure 4b shows simulated absorption spectrum of the $S_2(^1B_2)$ state with the displaced harmonic oscillator approximation at CASSCF level, and 1_0^1 is shown to be the strongest vibronic transition which agrees well with the experimental spectra. Figure 4b shows that the both spectral peak position and the profile is in very good agreement with experimental result. Anharmonic correction to the absorption spectrum of the $S_2(^1B_2)$ is negligible in the present simulation. In addition, Figs. 4c and 4d show the EOM-CCSD and TD-B3LYP simulated spectral profiles which are similar to Fig. 4b. Compare to the strongest vibronic transition 1_0^1, the 0-0 band intensity from EOM-CCSD simulation is stronger than that of the CASSCF simulation and the experiment. However, the highest peak is assigned as the 0-0 vibronic transition for the TD-B3LYP simulation.

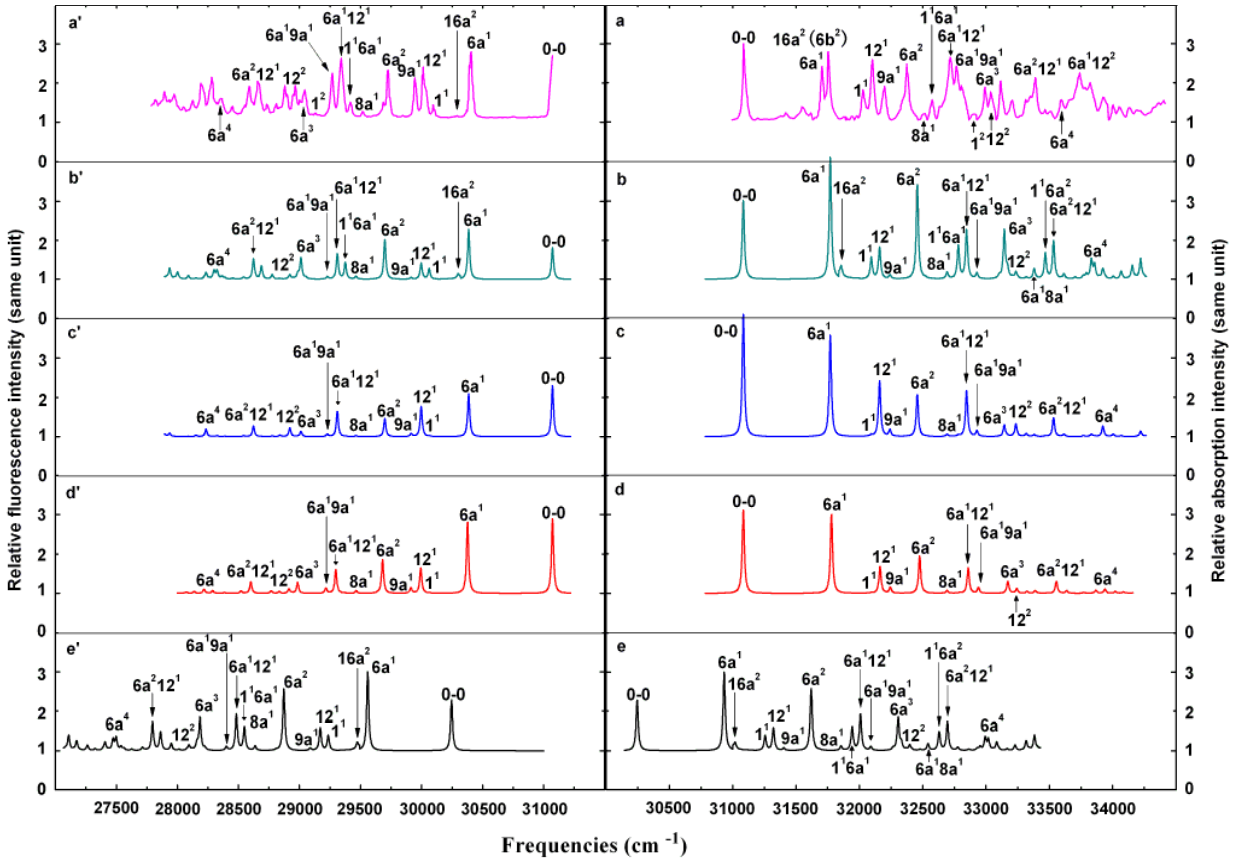

Figure 3. $S_1(^1B_1) \leftarrow S_0(^1A_1)$ absorption spectrum and $S_1(^1B_1) \rightarrow S_0(^1A_1)$ fluorescence spectrum of pyrimidine. Respectively, experimental data (a) and (a'); Simulated results with the present anharmonic correction, (b) and (b') CASSCF, (c) and (c') EOM-CCSD, (d) and (d') TD-B3LYP; Simulated results with the present harmonic oscillator approximation (e) and (e') CASSCF.

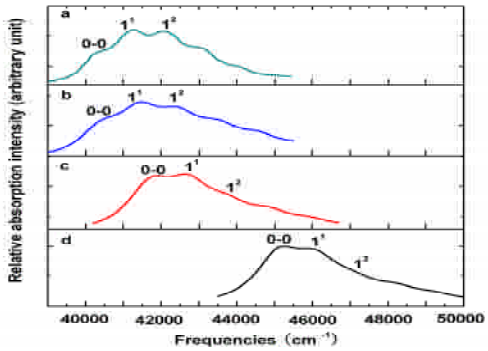

Figure 4. $S_2(^1B_2) \leftarrow S_0(^1A_1)$ absorption spectrum of pyrimidine simulated results with the present harmonic oscillator approximation. (a) Experimental data from Ref. [38], (b) CASSCF, (c) EOM-CCSD, (d)TD-B3LYP.

Concluding remarks

We have simulated absorption and fluorescence spectra for $S_1(^1B_1)$ state and the absorption spectrum for $S_2(^1B_2)$ state using harmonic and anharmonic oscillator approximation for pyrimidine molecule. We found that

the first-order anharmonic correction makes a significant contribution to band shift of spectra for S_1 state but it has no meaningful contribution to S_2 state. Franck-Condon simulations with including the first-order anharmonic correction show intensity enhancement of the absorption and intensity weakening of fluorescence for the adiabatic $S_1(^1B_1)$ state and this agrees well with experimental observation. Franck-Condon simulation of the absorption spectrum for the adiabatic $S_2(^1B_2)$ state shows good agreement with experimental observation without the anharmonic correction. We have optimized the equilibrium geometries of the electronic ground and the two lowest singlet excited states and then computed their 24-normal-mode frequencies that are all positive. All three electronic states have C_{2v} group symmetry. We confirmed that our calculation results are basically the same as those from high-level ab. initio calculation in the literatures. This means that the equilibrium geometries from the present calculation are accurate enough to be used for spectrum simulation. The electronic structure calculations confirmed that the $S_1(^1B_1)$ and $S_2(^1B_2)$ states have $n\pi^*$ and $\pi\pi^*$ configurations, respectively. Both vertical and adiabatic excitation energies of the $S_1(^1B_1)$ and $S_2(^1B_2)$ states are calculated and analyzed by comparing with various theoretical calculations and experimental results. Basically, even the best calculations for static adiabatic excitation energies of the $S_1(^1B_1)$ state differ from the experimental one, and the best calculation for static adiabatic excitation energy of $S_2(^1B_2)$ state agree exactly with the experimental one. This reflects that dynamic shift of excitation energies from anharmonic correction is significant for the $S_1(^1B_1)$ state, but not for $S_2(^1B_2)$ state. This is same as reorganization energy calculations that confirm 0.1 eV discrepancy between $\lambda_0(S_1)$ and $\lambda_{ex}(S_1)$ but little discrepancy between $\lambda_0(S_2)$ and $\lambda_{ex}(S_2)$. The present studies indicate that the frequency for each of the 9 total symmetric normal modes only slightly differs from one another for the three electronic states $S_0(^1A_1)$, $S_1(^1B_1)$ and $S_2(^1B_2)$. Furthermore, the transformation matrices that transfer geometric structure configuration from Jacobi to normal-mode coordinates for the three electronic states are also quite same for each of the nine total symmetric modes. Thus, displaced harmonic oscillator approximation is proved to be good approximation. In fact, Huang-Rhys factors directly indicate that the modes ν_{6a}, ν_1, and ν_{12} contribute S_1 absorption and fluorescence spectra, and S_2 absorption spectrum mostly, among which the main progression of S_1 bands comes from mode ν_{6a} and S_2 bands comes from mode ν_1. This agrees with experimental measurement. Although all ab initio CASSCF, CSPT2, CCSD/EOM-CCD and B3LYP/TD-B3LYP methods basically show good agreement with experimental results for vibronic spectra of pyrimidine molecule, the CASSCF shows the best agreement with experiment for weak-band intensities of vibronic spectra. This is because that CASSCF method provides equal footing calculation for electronic and excited states, and thus it produces the most accurate results for geometry differences between the ground and excited states. It should be emphasized that vibronic spectra is the most sensitive to the geometry difference, not absolute geometry for particular electronic state. The non-total symmetric vibrational mode 16a is taken into account in the present spectrum simulation within the distorted harmonic approximation and it devotes a weak band $16a^2$. The other non-total symmetric modes are negligible in spectrum simulation. The present first-order anharmonic corrections can only take into account diagonal part of anharmonicity so that it is not enough to correct detailed band shape in vibronic spectra. This is because that mode mixings due to off-diagonal part of anharmonicity are completely neglected as they belong to the second-order anharmonic corrections along with Duschinsky mode mixings. The conventional Herzberg-Teller effect of intensity borrowing from the other nontotally symmetric vibrational modes and possible nonadiabatic coupling due to conical intersection are not considered in the present studies as they both have little effect to totally symmetric vibrational modes.

2. “Excited State ab Initio and Franck Condon Simulation of S1 f S0 Fluorescence Excitation Spectra of p-, m-, and o-Difluorobenzenes,”
Q. Yang, R. He*,W. Shen, H. Li, M. Li, **C. Zhu*** and S. H. Lin
Published on J. Phys. Chem. A, 115, 14022 (2011)

Abstract

Although difluorobenzenes (DFBs) are well-known organic molecules to understand the electronic structure and spectroscopy of benzene and its derivatives, few theoretical investigations have been performed to simulate their fine spectra and assign their vibrational bands. In this work, the fluorescence excitation (FEX) spectra of the first excited singlet states for three DFBs molecules (para-, meta- and ortho-difluorobenzene) were simulated by the Franck-Condon calculations with the displaced harmonic oscillator approximation plus the distorted correction. The calculated results indicated that the spectral profiles of three DFBs are primarily described by the Franck_Condon progression of their totally symmetric vibrational modes. Specifically, it is found that modes v3 and v5 of para-DFB, v8 and v9 of meta-DFB, and ortho-DFB play the most important roles in the fluorescence spectra. By taking into account the contributions of the distorted effect, we could assign most of the dominant overtones from the nontotally symmetric vibrational modes, and the results agree well with the experimental assignments. Some inferred and unassigned vibrational transitions in experiment were confirmed according to the present calculated results. In addition, in the simulated fluorescence spectra, we tentatively assigned several combination bands with relative moderate intensity and weak vibrational lines which appeared in the experimental observations but the corresponding assignments were not given. The present work reproduced satisfactorily the experimental FEX spectra of p-, m-, and o-DFBs derivatives and provided a useful method to simulate the FEX spectra of dihalogenated benzene molecules.

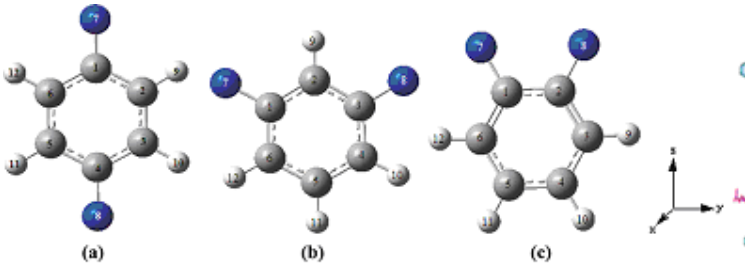

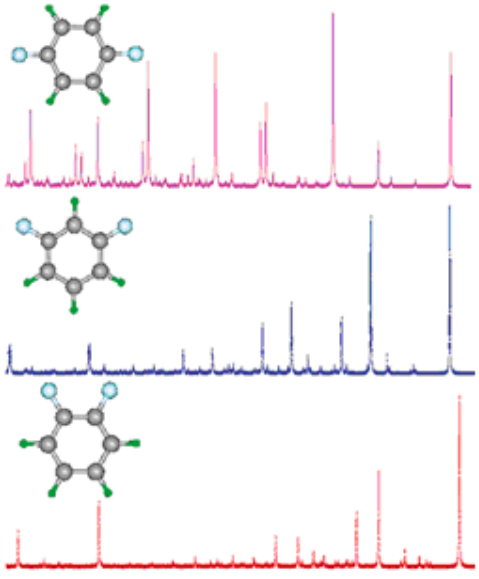

.

Figure 1. Molecular structure and atom numbering.
(a) p-;(b) m-; and (c) o-difluorobenzene

Fig2. Simulated spectra for figure 1

3. “The Role of the np* 1Au State in the Photoabsorption and Relaxation of Pyrazine,”
C.-K. Lin*, Y. Niu, **C. Zhu**, Z. Shuai, and S. H. Lin,
Published on Chem. Asian J., 6, 2977 (2011)

Abstract

The geometric, energetic, and spectroscopic properties of the ground state and the lowest four singlet excited states of pyrazine have been studied by using DFT/TD-DFT, CASSCF, CASPT2, and related quantum chemical calculations. The second singlet np* state, 1Au, which is conventionally regarded dark due to the dipole-forbidden 1Au !1Ag transition, has been investigated in detail. Our new simulation has shown that the state could be visible in the absorption spectrum by intensity borrowing from neighboring np* 1B3u and pp* 1B2u states through vibronic coupling. The scans on potential-energy surfaces further indicated that the 1Au state intersects with the 1B2u states near the equilibrium of the latter, thus implying its participation in the ultrafast relaxation.

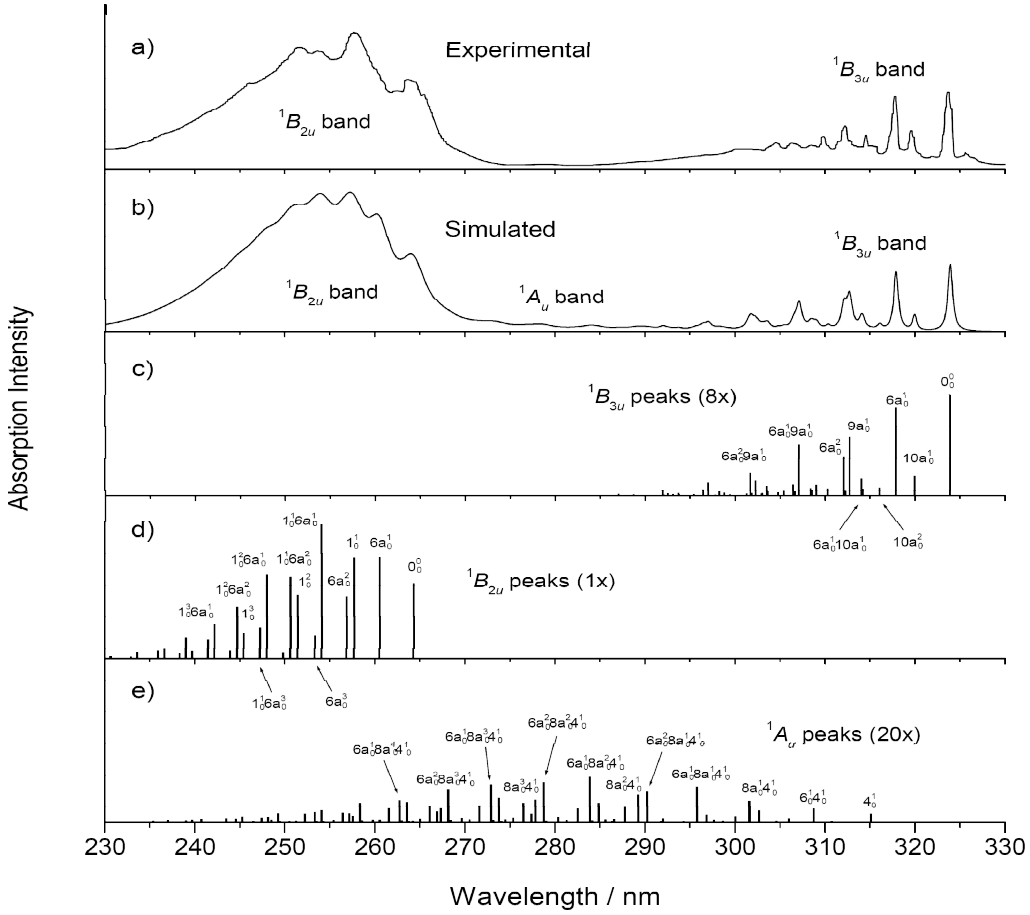

Figure. Absorption spectra of pyrazine covering 1B3u, 1B2u, and 1Au bands. a) Experimental UV spectroscopy. b) Simulated spectrum with peaks broadened by homogeneous dephasing. c), d), and e) Calculated peak intensities and assignments in these bands.

4 “Franck-Condon simulation of the A 1B2→X 1A1 dispersed fluorescence spectrum of fluorobenzene and its rate of the internal conversion,”
R. He, L. Yang, **C. Zhu***, M. Yamaki, Y-P. Lee, and S. H. Lin
Published on J. Chem. Phys. 134, 094313 (2011)

Abstract
By using three different hybrid exchange-correlation functionals containing 20%, 35%, and 50% of exact Hartree-Fock exchange of the density functional theory and its time-dependent extension plus the Hartree-Fock and the configuration interaction of single excitation methods, equilibrium geometries and their 30 vibrational-normal-mode frequencies of the ground $S_0(^1A_1)$ and the first excited $S_1(^1B_2)$ states of fluorobenzene were calculated. The dispersed fluorescence spectrum and internal conversion rate of the $A\ ^1B_2 \rightarrow X\ ^1A_1$ transition were simulated by Franck-Condon calculations within the displaced harmonic oscillator approximation plus anharmonic and distorted corrections. The simulated spectral profile is primarily described by the Franck-Condon progression from the ring-breathing modes v_9 and v_{10} which belong to totally symmetry modes. Anharmonic corrections simultaneously improve the intensity order of 9_1^0 and 10_1^0 bands and diminish 1_1^0 transition that is fairly strong in harmonic simulations. It is concluded that the amount of Hartree-Fock exchange does impact the geometries and vibrational frequencies of FB molecule, but not the relative intensities of the transitions. It is anharmonic corrections that make the relative intensities of the transitions in good agreement with experimental results. Distorted corrections could assign most of the dominant overtones of out-of-plane non-totally symmetry modes, and the results agree well with the experimental assignments. Furthermore, it was found that the internal conversion rate is dominated by three promoting modes that are computed with lowing symmetry to C_1. By choosing dephasing width as $10cm^{-1}$ that is consistent with spectral simulation, we obtained the lifetimes of the $A\ ^1B_2 \rightarrow X\ ^1A_1$ deexcitation as 11ns and 19ns, respectively from TD(B3LYP) and HF/CIS calculations in comparison with the experimental value 14.75ns.

Introduction
A main purpose of the present work focuses on the ab initio simulations of electronic spectra and internal conversion of Fluorbenzene. From theoretical point of view, these two processes are partly governed by the same Franck-Condon factor. In order to demonstrate how accurate simulation we can do for internal conversion process, we must show that the same ab initio level of calculation should perform well for electronic spectra. Time dependent density function method is used to calculate excited state in which the impact of Hartree-Fock exchange percentage in the hybrid functional is extensively investigated and discussed. In the present work, we first simulated the dispersed fluorescence electronic spectrum of FB following LIF excitation of the $^1B_2 \leftarrow ^1A_1$ by employing simple products of one-dimensional FC factors that corresponds to displaced harmonic oscillator approximation plus anharmonic and distorted effects. We believe that the DF spectral profile should be primarily described by the Franck-Condon progression in terms of the totally symmetry normal modes. Anharmonic correction to ground and excited states is assumed to be the same and thus their corrections are only to totally symmetry normal modes. The distorted effects that affect only non-totally symmetry normal modes should be small as it can be considered as diagonal-part correction of

Duschinsky mode-mixing matrix. We calculated the internal conversion (IC) rate of FB molecule following excitation of the $^1B_2 \leftarrow ^1A_1$ transition under the isolated molecular condition. Actually, the lifetimes and the radiationless transition rates from the single vibronic levels of S_1 state were measured under the collision-free condition by Abramson and the co-workers. Reported lifetimes and quantum yields of fluorescence come from 59 vibronic states, and the lifetime of 0-0 transition is about 14.8 ns. Radiationless transition involving two electronic states is partly governed by the nonadiabatic coupling that is determined by the off-diagonal matrix elements of the nuclear kinetic operators. This nonadiabatic coupling can be expressed in terms of series of normal-mode vibronic couplings which can be calculated by *ab initio* quantum mechanic methods and rate of internal conversion is usually sensitive to accuracy of those vibronic couplings.

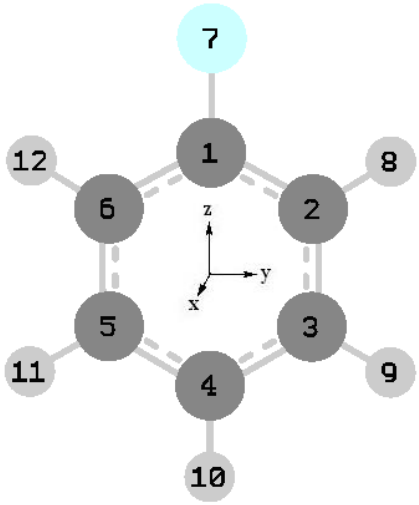

Fig. 1. The molecular structure and the atom numbering of fluorobenzene.

Franck-Condon simulation of DF spectrum

The dispersed fluorescence spectrum of the $A^1B_2 \rightarrow X^1A_1$ transition was measured and the detailed analyses were reported in the recent experiment studies, where the DF spectral profile is primarily described by the Franck-Condon progression in terms of the totally symmetry normal modes (a_1-type). Among these modes, ν_9 and ν_{10} are the main progression forming modes in the $^1B_2 \rightarrow ^1A_1$ fluorescence spectrum. The present calculations confirmed that modes ν_{10} and ν_9 have the largest Huang-Rhys factors (S = 0.420 and 0.408 for instance from B3LYP calculation and are assigned as the closest analogy to the ring-breathing modes in benzene. The modes ν_2, ν_3, ν_4 and ν_5, which are relative to the CH stretching and bending vibrations, have little contribution to FC factor as their Huang-Rhys factors are negligible small. Furthermore, the previous theoretical analysis also indicated that there exist very weak bands in DF spectrum, most of them are related to the non-totally symmetric normal modes, e.g. ν_{19} and ν_{16} (b_1 symmetry), that can be interpreted in terms of Duschinsky mixing.

In the present spectrum simulation, we utilized the unscaled vibrational frequencies calculated at the same levels of ab. initio method as was performed for optimizing the geometries of the electronic state. The band origin (0-0 transition) is set up to be zero (cm^{-1}) in the DF spectrum as it was adopted in experimental study . In order to simulate the experimental resolution of DF spectrum, Lorentzian broadening width is tested as γ_{ab} =10 cm^{-1} approximately. We know that this value contains not only the truly dephasing but also the

contribution from the instrumental broadening. The DF spectrum simulated from B3LYP, B3LYP-35, BHandHLYP, and CIS methods all show that the 0-0 transition is the strongest transition in the allowed $^1B_2 \rightarrow {}^1A_1$ electronic transition as shown in Fig.2 and Fig.3, and this agrees with experiment observation. All simulated DF spectra in Fig.2 and Fig.3 were performed in the framework of displaced harmonic and anharmonic oscillator approximation, respectively, in which the most prominent peaks have been assigned based on the present calculations in comparison with experimental data. It can be seen that all methods including CIS reproduce qualitatively the essential character of the observed spectrum.

According to the high resolution of experimental results performed by Butler *et al*., the DF spectrum is mostly assigned as the totally symmetric normal mode progressions; especially the mode ν_9 displays very strong intensity in the spectral profile and in the present B3LYP calculation the intensity of the vibronic line assigned as 9_1^0 fundamental is slightly underestimated; the intensity of 9_1^0 transition in experiment is about 70% of that of the 0-0 line, but that in the present calculation is about 50%. Harmonic Franck-Condon simulations in Fig.2 all indicate that the strongest and second strongest vibronic transitions are the 10_1^0 and 9_1^0 (after the 0-0 transition) which seems be reversed in comparison with the experiment result. When anhamonic corrections are added, simulations in Fig.3 from all methods except B3LYP-35 show that the 9_1^0 band is larger than 10_1^0 band in good agreement with experimental observation. Moreover, Harmonic Franck-Condon simulations in Fig.2 all indicate that there is strong peak in high energy region of DF spectra and this corresponds to 1_1^0 transition. When anhamonic corrections are added, simulations in Fig.3 from all methods show that 1_1^0 transition is diminished. This is because that Huang-Rhys factor 0.22 for mode ν_1 is significantly reduced with anharmonic correction. Within harmonic approximation vibartional displacement vector for mode ν_1 (CH stretching) is very large and even if CH bond lengths change very small from S_0 to S_1 state, Huang-Rhys factor is still as big as 0.22. However, anharmonic correction is also large and it effectively cancels out 1_1^0 transition. We can conclude that the amount of HF exchange (from 20% in B3LYP, 35% in B3LYP-35, 50% in BHandHLYP, and 100% in HF) does impact the geometries and vibrational frequencies of FB molecule, but not the relative intensities of the transitions. It is anharmonic corrections that influence the relative intensities of the transitions.

The experimental spectra in Figs. 2a and 3a show that the 10_1^0 transition strongly overlaps with 14_2^0 transition with a just split 15 cm^{-1}. According to the calculations based on the non-totally symmetric vibrational transitions , it is found that the 14_2^0 should be about one-third of the 10_1^0 in transition intensity. It should be also noticed that in the present simulation, the 10_2^0 transition and the combination band $10_1^0 14_2^0$ are nearly degenerate vibronic level pairs; the vibrational origins of 10_2^0 ($2\nu_{10}$=1637 cm^{-1}) and $10_1^0 14_2^0$ ($\nu_{10}+2\nu_{14}$=1613 cm^{-1}) are separated by 24 cm^{-1} from B3LYP calculation. This suggests there should be strong coupling between these two vibronic transitions (ν_1 and ν_{14}). On the other hand, from B3LYP calculation as shown in Figs. 2b and 3b we could assign the 10_2^0 (1637 cm^{-1}, that is, $2\nu_{10}$), 10_3^0 (2456 cm^{-1}), 9_2^0 (2036 cm^{-1}) and 9_3^0 (3054 cm^{-1}) vibronic transitions as four fundamentals located at 1613, 2434, 2016 and 3014 cm^{-1} in experiment, respectively. The detailed assignments based on the present analysis are shown in very good agreement with the experimental data. In the low energy region of DF spectrum, the experimental observation and the present B3LYP simulation agree well for the significant intensity assigned from normal mode ν_{11}, and this corresponds to Huang-Rhys factor S = 0.154 (from B3LYP). Intensity of 6_1^0 band in the

harmonic Franck-Condon simulation is lower than corresponding experiment intensity, but it is improved with anharmonic correction as shown in Fig.3. This fundamental ν_6 corresponds to the CF bond stretching in the present analysis. Furthermore, the experimental DF spectrum reported by Butler et al. showed that there are many moderate intensity peaks with the characteristics of combination between fundamental modes. Most of these transitions can be assigned based the present FC simulations. Figures 2a and 2b (3a and 3b) demonstrate how good agreement is for DF spectrum between experiment result and the present B3LYP simulation in terms of the ordering and positioning of these combination peaks as well as its intensity strengths, especially for extremely weak peak of the combination band of $9_2^0 6_1^0$ in the high frequency region is also reproduced correctly.

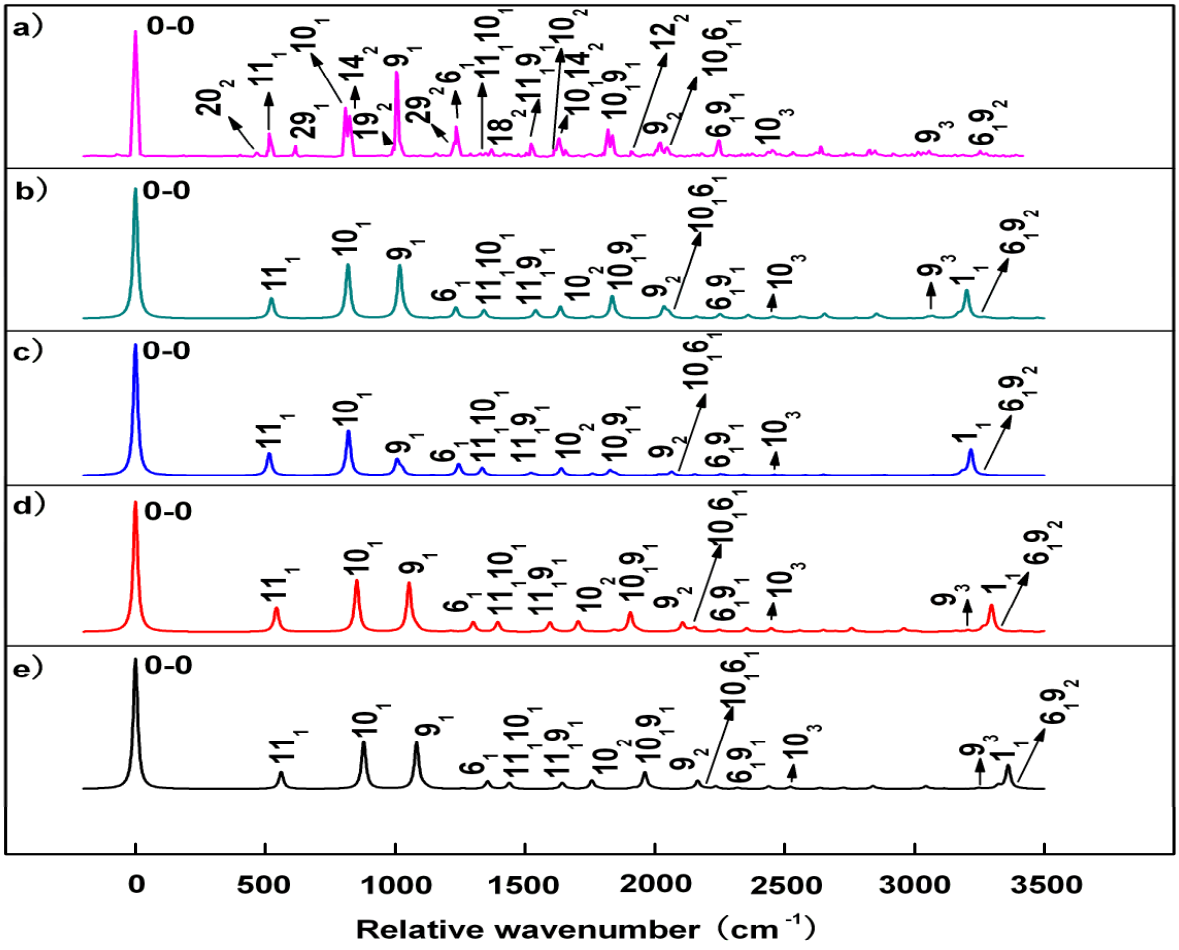

Fig. 2. The DF spectra of fluorobenzene from S_1 to S_0 transition calculated by harmonic FC simulation (the relative energy of the 0-0 transition is set up to be zero). (a) Experimental result. (b) (TD) B3LYP, (c) (TD) B3LYP-35, (d) (TD)BHandHLYP and (e) HF/CIS calculations.

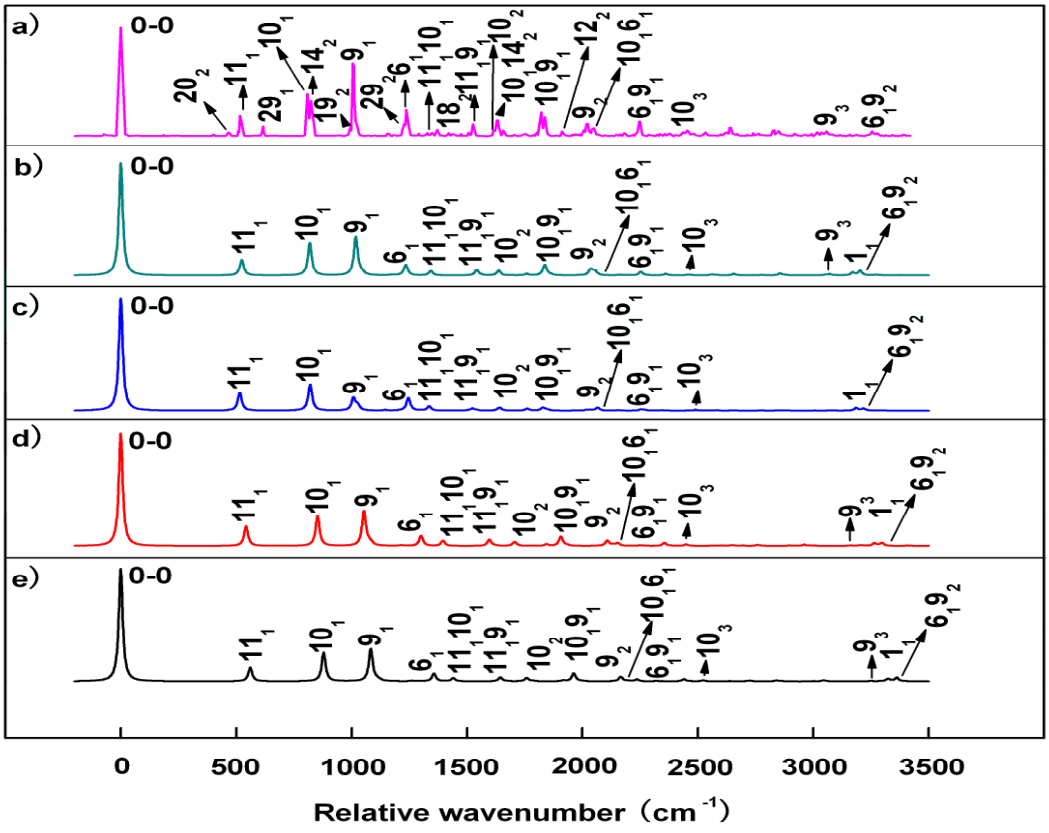

Fig.3 The same as Fig.4 but including anharmonic corrections.

Internal conversion and the lifetime of S_1 state

In order to compute internal conversion constant, we have to compute the nonadiabatic coupling matrix elements or vibronic couplings $\left\langle \Phi_f \left| \partial/\partial Q_l \right| \Phi_i \right\rangle$ (between S_0 and S_1 states) vertically at equilibrium geometry of S_1 state. At the equilibrium geometry of S_1 state calculated by two methods; (TD)B3LYP and HF/CIS, we employed CASSCF method for calculating nonadiabatic coupling matrix elements. We should mention that the equilibrium geometry optimized by (TD)B3LYP and HF/CIS methods may or may not correspond to true equilibrium optimized by CASSCF method, but on the other hand, vibronic couplings vary very slowly against change of geometry. We first computed vibronic couplings in Cartesian coordinate spaces and then transformed them into normal mode coordinates. However, we have to lowering group symmetry to C_1 in order to perform vibronic couplings by Molpro. We obtained 30 vibronic couplings among which there are only three modes at the same order of magnitude and the rest of them are negligibly small. These three modes do not have clear correspondence to modes obtained with C_{2V} group symmetry. Therefore, we can only label them according to order of frequency magnitude in C_1 symmetry, and they are 7th, 8th and 15th vibrational normal modes computed by CASSCF. Then, three vibronic couplings are converted to the

electronic part of the IC rate $\frac{1}{\hbar^2}\left|R_l(fi)\right|^2$. Two methods produce almost same the coupling matrix elements and its electronic part of the IC rate (see the coupling elements of the 7th normal mode are about 0.1482 and 0.1460 au., respectively from (TD) B3LYP and HF/CIS methods. This is because the optimized geometries of the excited state S_1 performed by two methods show small discrepancies, besides vibronic couplings vary slowly against change of geometry. .

Now we turn to compute the second part of IC rate of the transition $^1B_2 \rightarrow {}^1A_1$. The dephasing width γ_{if} is chosen as four values; 5 cm^{-1}, 10 cm^{-1}, 15 cm^{-1} and 20 cm^{-1}, so that calculated IC rate $k_{iv\rightarrow f}$ (or lifetime $\tau_l = 1/k_{iv\rightarrow f}(l)$) for single promoting mode *l* is function of dephasing width. Then, we can estimate total lifetime as

$$\tau_T = \frac{1}{\sum_l k_{iv\rightarrow f}(l)} = \frac{1}{\sum_l (1/\tau_l)}, \qquad (1)$$

where summation is over three promoting modes (7th, 8th and 15th in C_1 group symmetry). All results are given in Table I. Table I shows that calculated IC rate constants (the lifetimes) increase (decrease) with the increase of the dephasing width for each of the three promoting modes. For example, the TD(B3LYP) calculation indicates that the IC rate constant of mode 8th increases from 2.33×10^7 s^{-1} to 4.23×10^7 s^{-1} when dephasing width increases from 5 cm^{-1} to 10 cm^{-1}. It should be emphasized that the electronic part of IC rate $\frac{1}{\hbar^2}\left|R_l(fi)\right|^2$ is independent to dephasing width, and thus it is nuclear part of IC rate that is depending on dephasing width. How to determine dephasing width seems becoming a problem. If we use consistent choice of dephasing width for both calculations of DF spectrum and IC rate, we should choose the dephasing width as 10 cm^{-1} that was used for the DF spectrum simulation. At γ_{if} =10 cm^{-1}, the calculated total lifetimes of the decay $^1B_2 \rightarrow {}^1A_1$ are 11ns and 19ns, respectively from TD(B3LYP) and HF/CIS calculations in comparison with the experimental value 14.75 ± 0.34 ns (the lifetime of 0-0 deexciting transition is considered. The present calculations show very good agreement with experiment for IC rate constant (or decay lifetime). Taking both the approximations introduced in the present calculations and the experimental uncertainties into consideration, we conclude that the difference between the calculated and the experimental lifetimes (or the IC rates) is quite reasonable. We added anharmonic corrections to the second part of IC rate, and its results are the same as harmonic approximation.

TABLE I . The evaluated IC rate (k_{iv}) and lifetime (τ_l) for each of three promoting modes as well as the total lifetimes (τ_T) for the $^1B_2 \rightarrow {}^1A_1$ transition against different dephasing widths.

		TD(B3LYP)			HF/CIS			Exp.
□(cm^{-1})	mode	k_{iv} (10^7s^{-1})	τ_l (ns)	τ_T (ns)	k_{iv} (10^7s^{-1})	τ_l (ns)	τ_T (ns)	τ_T (ns)
5	7th	0.65	154	21	0.50	200	44	14.75 ± 0.34
	8th	2.33	43		0.85	118		
	15th	1.69	59		0.94	106		
10	7th	1.48	68	11	0.84	119	19	
	8th	4.23	24		2.42	41		
	15th	3.54	28		2.10	48		
15	7th	2.21	45	7.3	1.26	79	12	
	8th	6.34	16		3.64	27		
	15th	5.31	19		3.15	32		
20	7th	2.95	34	5.4	1.68	60	9.3	
	8th	8.45	12		4.85	21		
	15th	7.08	14		4.20	24		

Conclusion

In the present studies, we have simulated the DF spectrum and IC rate constant of fluorobenzne following excitation of the $^1B_2(S_1) \leftarrow {}^1A_1(S_0)$ transition from the S_1 state to S_0 state by using displaced harmonic oscillator approximation with and without including anharmonic and distorted correction. Starting from optimization of equilibrium geometries and the corresponding normal mode frequencies of S_0 and S_1 states, we obtained geometry parameters and frequencies generally in good agreement with experimental results [2, 4, 6] and the previous theoretical calculations. Three kinds of functionals (B3LYP, B3LYP-35, and BHandHLYP) with (TD)DFT method plus HF/CIS method were adopted for ab. initio calculations for ground and the first excited states. Based on accurate geometry parameters and frequencies calculated by these methods, we could compute displacement d_i between equilibrium geometries of S_0 and S_1 states and Huang-Rhys factor S_i accurately. Therefore, we are pretty confident about the present simulations on DF spectrum and IC rate constant. Displaced harmonic oscillator approximation presented very good examinations of the spectral profile and the assignments of the active fundamental normal modes in the DF spectrum of fluorobenzene, and its results basically agree well with the previous assignments studied in the literatures. Actually, the present calculations proved that totally symmetry vibrational modes dominate spectral profile and the assignments, especially described by the Franck-Condon progression from the ν_9 and ν_{10} modes and then we could also assign the dominant combination bands with moderate intensities, such as the bands $11_1^0 10_1^0$ and $10_1^0 14_2^0$, and so on. This is in good agreement with the experiment. Anharmonic corrections (which correct only totally symmetry modes) improved harmonic simulations simultaneously for the intensity order of 9_1^0 and 10_1^0 bands and diminishing 1_1^0 transition. Anharmonic corrections also

improved the other small bands from the rest of totally symmetry modes. We conclude that the amount of HF exchange (from 20% in B3LYP, 35% in B3LYP-35, 50% in BHandHLYP, and 100% in HF) does impact the geometries and vibrational frequencies of FB molecule, but not the relative intensities of the transitions. It is anharmonic corrections that influence the relative intensities of the transitions.

We considered using the distorted corrections (which only correct non-totally symmetry modes) to explain the overtones of out-of-plane vibrations which arise from the non-totally symmetric vibrational modes. The present calculations indicated that some of small peaks in the DF spectrum are due to contributions from the distorted effect. However, its contributions to spectra are basically small in comparison with totally symmetry modes.

By using the CASSCF method, we calculated the electronic matrix elements of nonadiabatic coupling between the S_0 and S_1 states and then we computed the single vibronic level internal conversion rate of the $^1B_2(S_1) \rightarrow {}^1A_1(S_0)$ transition within the collision-free condition. It was found that the IC rate is sensitive to the dephasing width. Around γ_{if} =10 cm^{-1} that is adopted for spectrum simulation, the calculated total lifetimes of this decay are in good agreement with the experimental observation.

5. “A quasiclassical trajectory study of reactive scattering on an analytical potential energy surface for GeH2 system,”

L. Zhang, C. R. Zhu, G. Jiang, **C. Zhu*** , and Z. H. Zhu

Published on Journal of Theoretical and Computational Chemistry 10, 147(2011)

Abstract

A quasiclassical trajectory method is employed to study reaction Ge + H2 (v=0, j=0) reaction and reverse reaction H +GeH (v=0, j=0) on a analytical potential energy surface which is obtained from simplified many-body expansion method with fitting to B3P86/CC-pVTZ calculations around a global minimum and a long range van de Waals well plus spectroscopy data from diatomic molecules GeH and H2. Reaction probabilities from both reaction and reverse reaction are calculated. Dominant reaction is Ge + H2 (v=0, j=0)□ GeH2 complex forming reaction, and its cross sectoi n is ten times bigger than that of complex forming reaction from the reverse reaction. There is no threshold effect for complex forming reaction and the cross sections for both complex-forming reactions decrease with increase of collision energy. Life time of complex is shown to be decreasing with increase of collision energy. Dominant reverse reaction is reaction H +GeH (v=0,j=0) □ Ge + H2, reaction probability decreases with increase of collision energy and differential cross section shows that this reverse reaction has almost equal angular distribution at low collision energy and mostly forward scattering at high collision energy.

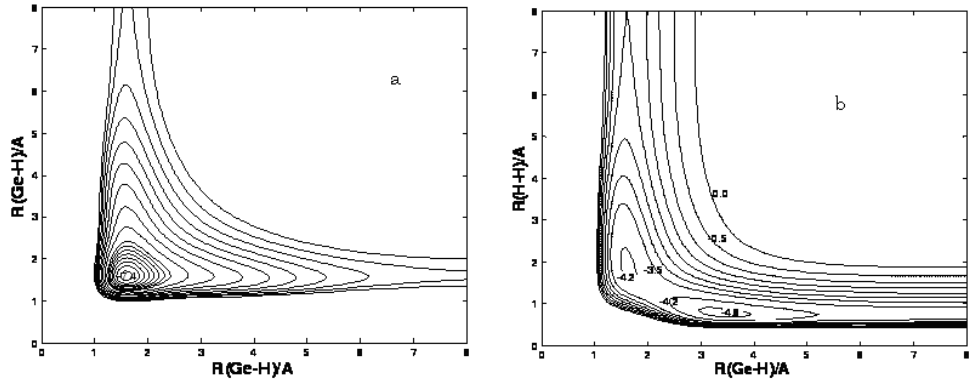

Fig.1. Potential contour plots (a) at a fixed angle = 90.628° for Ge-H and H-Ge bonds stretching and (b) at fixed angle (<GeHH)=180° for Ge-H and H-H bonds stretching.

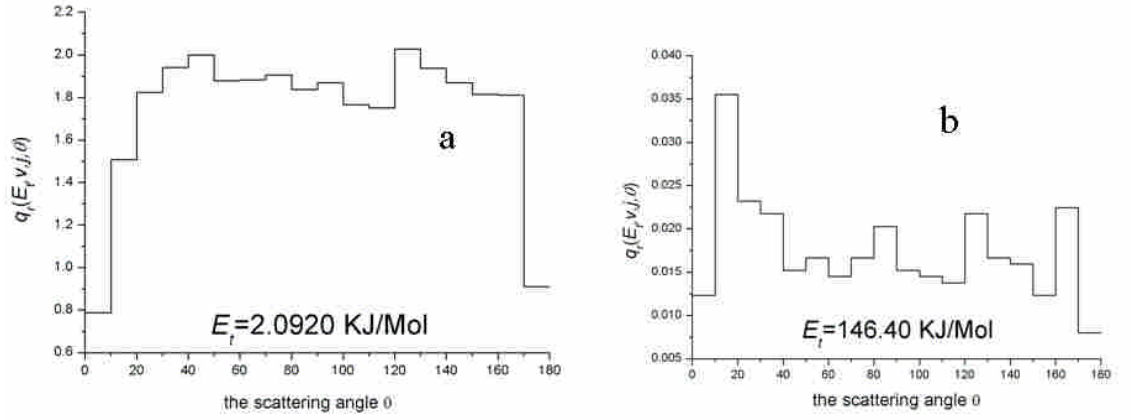

Fig.2. Differential cross sections (DCSs) for reaction H + GeH(v = 0, j = 0) → Ge + H_2 with translational collision energies (a) E_t = 2.0920kJ/mol and (b) E_t = 146.40kJ/mol.

6. “Symmetry forbidden vibronic spectra and internal conversion in benzene,”
J. Li, C-K. Lin*,X. Y. Li, **C. Zhu** and S. H. Lin
Published on Phys.Chem.Chem.Phys.12, (2010)

Abstract
The spectra of symmetry-forbidden transitions and internal conversion were investigated in the present work. Temperature dependence was taken into account for the spectra simulation. The vibronic coupling, essential in the two processes, was calculated based on the Herzberg–Teller theory within the Born–Oppenheimer approximation. The approach was employed for the symmetry-forbidden absorption/fluorescence, and internal conversion between 11A1g and 11B2u states in benzene. Vibrational frequencies, normal coordinates, electronic transition dipole moments, and non-adiabatic coupling matrix elements were obtained by ab initio quantum chemical methods. The main peaks, along with the weak peaks, were in good agreement with the observed ones. The rate constant of the 11A1g ’ 11B2u internal conversion was estimated within the order of 103 s_1. This could be regarded as the lower limit (about 4.8 _ 103 s_1) of the internal conversion. It is stressed that the distortion effect was taken into account both in the symmetry-forbidden absorption/fluorescence, and the rate constants of internal conversion in the present work. The distortion effects complicate the spectra and increase the rate constants of internal conversion.

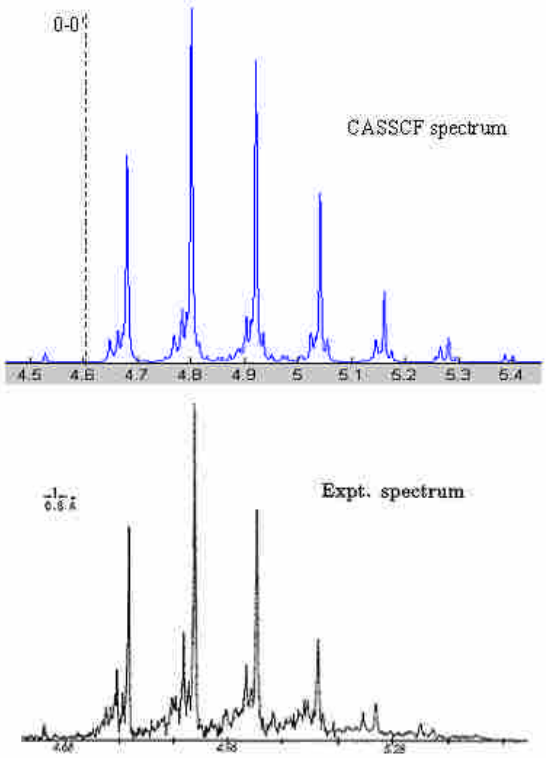

Fig. 1. The spectrum for the a bsorption $1^1A_{1g} \rightarrow 1^1B_{2u}$ in benzene

Table 1. Calculations of the rates of internal conversion $1^1A_{1g} \leftarrow 1^1B_{2u}$

	Q_{14}	Q_{15}
$it'(\mathrm{cm}/2\pi)$	9.78×10^{-4}	9.85×10^{-4}
$\langle\Phi_k\|\partial/\partial Q_j\|\Phi_i\rangle$	0.2843	-0.4042
$\prod_j g_j(t')$	2.2261	2.7012
W (s^{-1})	2.85×10^{3}	1.91×10^{3}

7. “Anharmonic Franck–Condon simulation of the absorption and fluorescence spectra for the low-lying S1 and S2 excited states of pyridine,”
H. Wang, **C. Zhu***, J. G. Yu, and S. H. Lin
Published on J. Phys. Chem. A, , 113, 14407 (2009)

Abstract
Anharmonic effects of the absorption and fluorescence spectra of pyridine molecule are studied and analyzed for the two-low lying singlet excited states $S_1(^1B_1)$ and $S_2(^1B_2)$. The complete active space self-consistent field (CASSCF) method is utilized to compute equilibrium geometries and all 27 vibrational normal-mode frequencies for the ground state and the two excited states. The present calculations show that the frequency differences between the ground and two excited states are small for the ten totally symmetric vibrational modes so that the displaced oscillator approximation can be used for spectrum simulations. The Franck-Condon factors within harmonic approximation basically grasp the main features of molecular spectra, but simulated 0-0 transition energy position and spectrum band shapes are not satisfactorily good for $S_1(^1B_1)$ absorption and fluorescence spectra in comparison with experiment observation. As the first-order anharmonic correction added to Franck-Condon factors, both spectrum positions and band shapes can be simultaneously improved for both absorption and fluorescence spectra. It is concluded that the present anharmonic correction produces a significant dynamic shifts for spectrum positions and improves spectrum band shapes as well. The detailed structures of absorption spectrum of $S_2(^1B_2)$ state observed from experiment can be also reproduced with anharmonic Franck-Condon simulation and these were not shown up in the harmonic Franck-Condon simulation with either distorted or Duschinsky effects in the literatures.

Introduction
Theoretical simulation of molecular dynamics and spectroscopy starts from Born-Oppenheimer approximation, within which electronically ground-state and excited-state wave functions are calculated with further approximation methods from conventional Ab. initio quantum chemistry. Within Born-Oppenheimer approximation, the Franck–Condon (FC) overlap integrals of vibrational wave functions belonging to two different electronic states are essential quantities in the theoretical description for the vibronic structure of electronic spectra like UV absorption, fluorescence, and other nonradiative processes like electronic and energy transfer. Exact calculation for multidimensional FC overlap integrals is not practical for many-atom systems. Harmonic approximation with normal-mode analysis is commonly utilized to interpret experimental spectroscopy and anharmonic correction to harmonic approximation is sometime necessary for making improvement of simulation. Under harmonic and/or anharmonic approximation, further approximations can be classified regarding to difference between ground-state and excited-state vibrational normarl modes as displaced oscillator approximation, distorted oscillator approximation, and normal mode-mixing with including Duschinsky effect. Various analytical and numerical methods are developed to compute FC overlap integrals with applications to molecular spectroscopy and energy and electron transfer processes.

There are a large number of computational studies on equilibrium geometries, vibrational frequencies, and spectra for ground state and low-lying excited states of pyridine. Franck-Condon simulations within displaced harmonic oscillator approximation including distorted effects were performed for S_1 and S_2 absorption spectra,

and simulations including Duschinsky effect were performed as well. Both distorted and Duschinsky effects seem small for absorption spectra of pyridine. It is our motivation in the present studies to investigate anharmonic effects on the absorption and fluorescence spectra for pyridine, especially the first-order anharmonic approximation that is the leading contribution to spectra is actually performed. With analytical formulation of absorption and fluorescence coefficients as well as computational formulas for the certain anharmonic constants, we have a powerful tool to demonstrate a distinguished contribution, in which the shifts of spectra, relative intensity and structure changes of spectra are simulated as a direct consequence of the first-order anharmonic correction with respect to harmonic Franck-Condon simulation.

The understanding of anharmonic effect on spectra from analytical formulation is of importance in which it not only gives direct insight into phenomena occurring in spectra but also provides a way to clearly classify static with dynamic contributions to spectra in which the conventional numerical method is hard to distinguish various effects in spectra. As theoretical calculations for adiabatic potential energy differences between excited-stated and ground-state equilibrium geometries seems much larger than experimental observation of $0\rightarrow 0$ excitation energy, we demonstrate in this paper that the discrepancy between theoretical simulations and experimental observation is actually due to the first-order anharmonic correction for the S_1 absorption and fluorescence spectra of pyridine. The certain surviving structures observed in the broaden band S_2 absorption spectrum also show up within the first-order anharmonic correction.

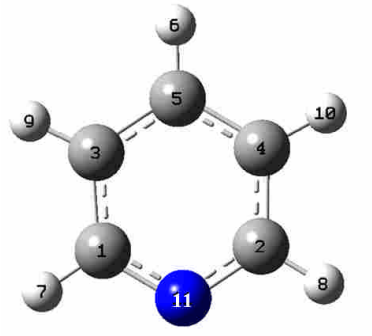

Fig. 1. Atom numbering for pyridine.

Absorption spectra

We simulate the absorption spectra for both $S_1(^1B_1)$ and $S_2(^1B_2)$ states as shown in Figs. 2 and 4, respectively, and the fluorescence emission spectrum for $S_1(^1B_1)$ state as shown in Fig. 3 within both displaced harmonic and displaced anharmonic oscillator approximations. The temperature is taken as 298K in the simulations as the experimental spectra were obtained at room temperature. The present CASSCF frequencies in Table 2 are utilized in both absorption and fluorescence spectrum simulations for the two excited states. The present dephasing constant γ_{ba} are chosen as 25 cm^{-1} and 600 cm^{-1} for the excited states $S_1(^1B_1)$ and $S_2(^1B_2)$, respectively.

The main progressions of vibrational bands for the S_1 absorption and fluorescence spectra come from ν_{6a} mode accompanied by sub-contributions from modes ν_1 and ν_{12}. The Huang-Rhys factors for the modes ν_{6a}, ν_1, and ν_{12} are 1.41, 0.5 and 0.54, respectively, which produce the main contribution for both absorption spectrum

in Fig. 2 and fluorescence spectrum in Fig.3 within the observed spectrum band region. The overall progressions of spectra are reproduced by harmonic oscillator approximation as shown in Fig. 2d and Fig.3d. We utilize the best static excitation energy $|\omega_{ab}| = 4.41\,\text{eV}$ for the S_1 state, the peak position of the 0-0 excitation from harmonic oscillator approximation shows a big discrepancy with experiment observation for absorption spectrum (compare Fig. 2a with 2d) and for fluorescence spectrum (compare Fig.3a with 3d). When we add anharmonic correction χ_{jj} with $\frac{\chi_0}{-\sum_j (\chi_{jj}/4)} \approx \frac{2}{3}$ estimated from B3LYP method, we obtain anharmonic quantities η_i, signs of which are determined by sign of $\chi_{jj}a_{j3}$. In this way, we obtain spectrum shift $\Omega_0 = -523\,\text{cm}^{-1}$ in which the minus corresponds to red shift of spectrum as can be seen from Fig.2c and Fig.3c. In fact, the anharmonic constants χ_{jj} computed from Gaussian are not accurate enough in which the experiment values for the highest three vibrational-normal modes (over 3300cm^{-1}) are two to three times bigger than computed ones. With scaling scheme that is widely used in harmonic frequency calculation, we make a factor of 3 to all anharmonic constants χ_{jj} so that η_i becomes $\sqrt{3}\eta_i$ which leads to spectrum shift $\Omega_0 = -\sqrt{3} * 523\,\text{cm}^{-1}$. This results in the correct peak position for 0-0 transition as well as the other peaks in spectra depicted in Fig. 2b for absorption and Fig. 3b for fluorescence. We conclude that $\Omega_0 = -0.11\text{eV}$ is dynamic correction to static adiabatic excitation energy $|\omega_{ab}| = 4.41\,\text{eV}$. At the same time, the anharmonic quantity $\eta_{6a} = 0.08$ makes effective the Huang-Rhys factor for absorption as $S'_{6a} = S_{6a}(1+3\eta_{6a}) = 1.75$ and for fluorescence as $S'_{6a} = S_{6a}(1-3\eta_{6a}) = 1.1$, which leads to v_{6a} transition profiles and relative intensity changes as well, as illustrated in Fig. 2c and Fig. 3c. With factor of three scaling to anharmonic constants χ_{jj}, we finally simulate absorption spectrum in Fig.2b and fluorescence spectrum in Fig.3b that is in good agreement with experiment. The first-order anharmonic correction makes both spectra shift and profile change simultaneously in the right direction in comparison with experimental absorption and fluorescence spectra for S_1 state. It should be noted that the CASSCF frequencies are utilized in spectrum simulations and overall spectra band widths are wider than experiment ones mainly due to discrepancy of 6a-mode frequency between calculation and experiment (about 45 cm^{-1} difference).

Let us now start to analyze the S_2 absorption spectrum. The largest Huang-Rhys factor for the $S_2(^1B_2)$ state is 1.14 for vibrational mode v_1 accompanied by the other two, 0.116 for the mode v_{6a} and 0.118 for mode v_{12}. The highest peak from experimental is assigned as the 1_0^2 vibronic transition, while the present calculation shows 1_0^1 as the strongest transition. The present harmonic displaced oscillator approximation simulates absorption spectrum depicted in Fig. 4d in which the spectrum profile has two shoulders similar to what Cai and Reimers simulated by including the Duschinsky effects. This probably means that Duschinsky effects are not important. When we add anharmonic correction, the two shoulders disappear and profile structure around peak position turns to be in accordance with experimental spectrum shape (compare Fig.4a with Fig.4c). The

spectrum shift is now equal to $\Omega_0 = +281\,\mathrm{cm}^{-1}$ in which the plus corresponds to blue shift of spectrum as can be seen from Fig.4c. With scaling of a factor of 2 to all anhramonic constants χ_{jj} in Table 2, the spectrum shift becomes $\Omega_0 = \sqrt{2} * 281\,\mathrm{cm}^{-1} = 0.04eV$ which is in correct direction in comparison with experiment 0-0 transition. Similarly, spectrum shape around peak position is getting more close to experimental profile. As $\eta_1 = 0.066\mathrm{cm}^{-1}$ for mode 1, it is still too small to make effective Huang-Rhys factor $S_1' = S_1(1+3\eta_{6a}) = 1.34$ larger than 2 which is necessary for identifying 1_0^2 vibronic transition as the strongest one. Nevertheless, the present anharmonic correction make spectrum shift and profile change in the right direction in comparison with experiment observation. It should be noted that the harmonic displaced oscillator approximation with including distorted effect, and it did not show up detail structure around peak position. We could conclude that the first-order anharmonic correction does make an important contribution to absorption spectrum for S_2 state.

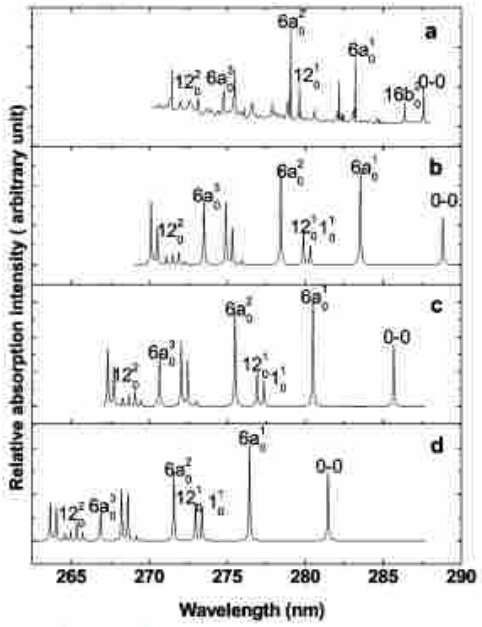

Figure 2. $S_1(^1B_1)$—$S_0(^1A_1)$ absorption spectrum of pyridine and the simulation with eq 2.10. (a) Experimental data from ref 36. Spectrum simulated from the present anharmonic correction with (b) $\sqrt{3}\bar{\eta}_i$ and (c) η_i for all 10 totalsymmetry modes. (d) Spectrum simulated from the present harmonic oscillator approximation.

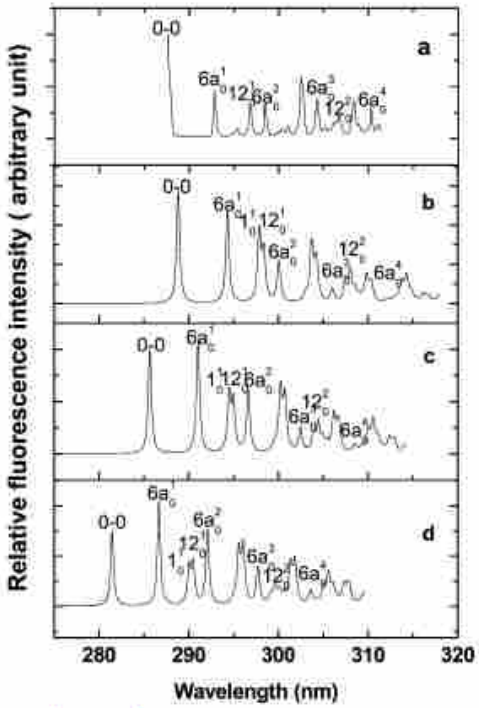

Figure 3. $S_1(^1B_1)$—$S_0(^1A_1)$ fluorescence spectrum of pyridine and the simulation with eq 2.11. (a) Experimental data from ref 38. Spectrum simulated from the present anharmonic correction with (b) $\sqrt{3}\bar{\eta}_i$ and (c) η_i for all 10 total symmetry modes. (d) Spectrum simulated from the present harmonic oscillator approximation.

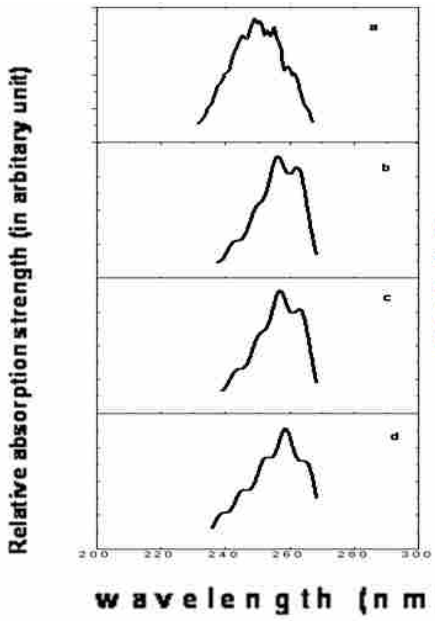

Figure 4. $S_2(^1B_2)$←$S_0(^1A_1)$ absorption spectrum of pyridine and the simulation with eq 2.10. (a) Experimental data from ref 39. Spectrum simulated from the present anharmonic correction with (b) $\sqrt{2}\bar{\eta}_i$ and (c) η_i for all 10 total symmetry modes. (d) Spectrum simulated from the present harmonic oscillator approximation.

Concluding remarks

We have simulated both absorption and fluorescence spectra for S_1 state and absorption spectrum for S_2 state of pyridine by using both displaced harmonic and anharmonic oscillator approximation. We found that the first-order anharmonic correction make a significant contribution to band shift and profile changes of spectra for pyridine molecule. We have utilized both CASSCF method to compute the equilibrium geometries of the electronic ground and the lowest two-singlet excited states of pyridine with their 27-normal-mode frequencies. All three electronic states show a C_{2v} symmetry, and calculation results are basically the same as those from high-level Ab. initio calculation in the literatures. This makes that the equilibrium geometries from the present calculation are accurate enough to be used for spectrum simulations.

The electronic structure calculations confirm that the $S_1(^1B_1)$ and $S_2(^1B_2)$ states have nπ* and ππ* configurations, respectively. Both cited vertical and calculated adiabatic excitation energies of the $S_1(^1B_1)$ and $S_2(^1B_2)$ states are discussed and analyzed by cross comparison with various theoretical calculations and experimental results. Basically, even the best calculations for static adiabatic excitation energies of the $S_1(^1B_{3u})$ and $S_2(^1B_{2u})$ states differ from the experimental ones. With the present anharmonic correction computed from B3LYP and MP2 methods, we could extract the excitation energies from dynamic effect so that experiment excitation energies should include both the calculated static excitation energies and dynamic shift.

The present studies indicate that, for the three electronic states of pyridine, $S_0(^1A_1)$, $S_1(^1B_1)$ and $S_2(^1B_2)$, the frequencies of the ten totally symmetric normal modes only slightly differ from one anther. Furthermore, we obtain the transformation matrices that transfer system from Jacobi to normal-mode coordinates for the three electronic states and we find that the corresponding matrices for ten totally symmetric modes are quite similar. Thus, displaced harmonic and anharmonic oscillator approximations can be used for simulation. In fact, from Huang-Rhys factors we conclude that the modes ν_{6a}, ν_1, and ν_{12} contribute S_1 absorption and fluorescence spectra and S_2 absorption spectrum mostly, among which the main progression of S_1 bands comes from mode ν_{6a} and S_2 bands comes from mode ν_1. This agrees with experimental measurement. It should be mentioned

again that the present first-order anharmonic corrections can only take into account diagonal part of anharmonicity, and mode mixings (differ from Duschinsky mode mixings) due to off-diagonal part of anharmonicity are completely neglected as they belong to the second-order anharmonic corrections. The conventional Herzberg-Teller effect of intensity borrowing from the other non-totally symmetric vibrational modes and possible nonadiabatic coupling due to conical intersection are not considered in the present studies as the both have little effect to totally symmetric vibrational modes.

In conclusion, simulations of absorption and fluorescence spectra from the adiabatic $S_1(^1B_1)$ and $S_2(^1B_2)$ states show good agreement with experimental observation with taking into account the first-order anharmonic correction to harmonic Franck-Condon simulation. Anharmonic correction plays the most significant role for pyridine spectra in comparison with distorted effects or/and Duschinsky effects.

8. “Analytical semilcassical theory for general nonadiabatic transition and tunneling,”
Published on Phys. Scr. 80, 048114 (2009)
C. Zhu

Abstract
Semiclassical solution of general two-state nonadiabatic transition and tunneling is found analytically within the WKB semiclassical framework associated with the Stokes phenomenon in mathematics. Nonadiabatic scattering matrix is determined by one complex quantity, called as the Stokes constant, which can be directly connected to the complex transition points of the WKB solution. An accurate and compact analytical solution is found for this Stokes constant which is function of three parameters, one of them corresponds to the diabatic-to-adaiabtic transformation angle that is interpreted as a type of nonadiabatic transition. Numerical examples demonstrate that the present unified analytical semilcassical theory works very well for both nonadiabatic transition and nonadiabatic tunneling. The present analytical semiclaasical method can be a very powerful tool in application of multidimensional nonadiabatic dynamic processes.

Introduction
The Born-Oppenheimer (BO) approximation [1] that separates the electronic motion with the nuclear motion made an outstanding step toward solving the Schrödinger equation for complicated molecular systems. There are numerous developments and successful applications of electronic structure and molecular dynamics methods for electronically adiabatic motions on the BO potential energy surfaces. Electronically nonadiabatic or non-Born-Oppenheimer transitions which arise from a break down of the BO approximation are involved in photochemistry, laser induced chemistry, electronic energy transfer, chemical reaction, electronic transfer, non-radiative transitions, and so on. At present and even in the near future an exact quantum mechanical treatment is impractical for large molecular systems for the both BO and Non-BO molecular dynamics. Semiclassical methods, mixed quantum-classical methods, and mean-field classical methods must be employed for solving the molecular dynamics Schrödinger equation. This review paper is focused on an analytical semiclassical theory for general nonadiabatic transition and nonadiabatic tunneling. As is well-known, nonadiabatic transition and nonadiabatic tunneling zones are occurred at very localized regions of entire electronically configurations in which molecular dynamics is mostly governed by the BO approximation, it is especially suitable for applying an analytical semicalssical method to deal with these localized transitions. An analytical semiclassical solution is very useful to understand intermediate dynamics and to analyze associated quantum effects, and it can be also applied as a connection matrix to connect wave functions at various boundary conditions associated with various coordinated systems. It can greatly enhance numerical performance by combining with various other molecular dynamic methods.

A motivation of the present review article is to reformulate the unified analytical semiclassical theory within the complex WKB method associate with the Stokes phenomenon in mathematics. For general two-state nonadiabatic scattering problems the coupled Schrödinger equations in the diabatic representation are written as

$$\left(-\frac{\hbar^2}{2\mu}\frac{d^2}{dR^2}+\begin{bmatrix}V_{11}(R) & V_{12}(R)\\ V_{21}(R) & V_{22}(R)\end{bmatrix}\right)\begin{pmatrix}\psi_1(R)\\ \psi_2(R)\end{pmatrix}=E\begin{pmatrix}\psi_1(R)\\ \psi_2(R)\end{pmatrix}, \tag{1}$$

where μ is the reduced mass of the system and R is a spatial coordinate that is general one-dimensional curved coordinate in a multidimensional potential energy surface (along trajectory for instance). Equation (1) can be transformed into the adiabatic representation by

$$U(\theta(R)) = \begin{bmatrix} \cos\theta(R) & \sin\theta(R) \\ -\sin\theta(R) & \cos\theta(R) \end{bmatrix}, \tag{2}$$

where the diabatic-to-adiabatic transformation angle is given by

$$\tan(2\theta(R)) = \frac{2V_{12}(R)}{V_{22}(R) - V_{11}(R)}. \tag{3}$$

Two adiabatic potential energy surfaces are defined by

$$E_1(R) = \frac{1}{2}(V_{22}(R) + V_{11}(R)) - \frac{1}{2}\sqrt{(V_{22}(R) - V_{11}(R))^2 + 4V_{12}^2(R)} \tag{4}$$

and

$$E_2(R) = \frac{1}{2}(V_{22}(R) + V_{11}(R)) + \frac{1}{2}\sqrt{(V_{22}(R) - V_{11}(R))^2 + 4V_{12}^2(R)}. \tag{5}$$

Thus, the coupled Schrödinger equations in the adiabatic representation can be obtained (not necessary given here), and the WKB-type of wave functions can be obtained as

$$\psi_1(R) = \frac{A_1}{\sqrt{p_1(R)}} \exp\left(i\int_{T_1}^{R} p_1(R)dR - i\frac{\pi}{4} \right) + \frac{B_1}{\sqrt{p_1(R)}} \exp\left(-i\int_{T_1}^{R} p_1(R)dR + i\frac{\pi}{4} \right) \tag{6}$$

and

$$\psi_2(R) = \frac{A_2}{\sqrt{p_2(R)}} \exp\left(i\int_{T_2}^{R} p_2(R)dR - i\frac{\pi}{4} \right) + \frac{B_2}{\sqrt{p_2(R)}} \exp\left(-i\int_{T_2}^{R} p_2(R)dR + i\frac{\pi}{4} \right), \tag{7}$$

where T_i (i=1,2) is the turning point on the adiabatic potential curve E_i(R) with

$$p_i(R) = \frac{\sqrt{2\mu}}{\hbar}\sqrt{E - E_i(R)}. \tag{8}$$

A reduced scattering matrix which includes all necessary information of nonadiabatic dynamics is defined by

$$\begin{pmatrix} A_1 \\ A_2 \end{pmatrix} \equiv S^R \begin{pmatrix} B_1 \\ B_2 \end{pmatrix} = \begin{pmatrix} S_{11}^R & S_{12}^R \\ S_{21}^R & S_{22}^R \end{pmatrix} \begin{pmatrix} B_1 \\ B_2 \end{pmatrix}, \tag{9}$$

where A_1 and A_2 (B_1 and B_2) represent amplitudes of the outgoing (incoming) WKB wave functions in Eqs. (6) and (7). This reduced matrix is semiclassically determined by two potential energy surfaces and its coupling in nonadiabtic transition zone as shown in Fig.1. Further analysis can prove that the reduced scattering matrix can be expressed in terms of one complex quantity U_1,

$$S^R = \begin{pmatrix} 1 + U_1 U_2 & -U_2 \\ -U_2 & 1 - U_1^* U_2 \end{pmatrix}, \tag{10}$$

where

$$U_2 = \frac{U_1 - U_1^*}{1 + U_1^* U_1}. \tag{11}$$

Equations (10) and (11) are actually proved for the LZS model in Ref. 26, and it is assumed here that it holds

semiclassically for general two-state nonadiabatic dynamics processes. Therefore, the main goal in the present paper is to find an analytical solution for this complex quantity U_1 that is called the Stokes constant in mathematics. Before starting mathematical derivation, it would be wise to ask what kind potential parameter determines nonadiabatic transition type. The answer actually comes from the diabatic-to-adiabatic transformation angle in Eqs. (2) and (3). Since nonadiabatic transition is occurred at a localized region, the most possible region is taken place at the complex crossing point R^* defined by

$$0 = E_2(R^*) - E_1(R^*) = \sqrt{\left(V_{22}(R^*) - V_{11}(R^*)\right)^2 + 4V_{12}^2(R^*)}. \tag{12}$$

For the LZS model of the two-state linear curve crossing problem, inserting a real part of the complex crossing point $\mathrm{Re}(R^*) = R_0$ into Eq. (3) that leads to

$$\tan(2\theta(R_0)) = \infty \Rightarrow \theta(R_0) = \frac{\pi}{4}, \quad \text{for the LZS model.} \tag{13}$$

Then, its diabatic-to-adiabatic transformation matrix in Eq. (2) shows the maximum mixing of the two representations because the two diagonal elements are equal the two off-diagonal elements in magnitude: $\cos(\pi/4) = \sin(\pi/4)$. For the RZ model of the two-state linear noncrossing problem, we have

$$\tan(2\theta(R_0)) = 1 \Rightarrow \theta(R_0) = \frac{\pi}{8}, \quad \text{for the RZ model.} \tag{14}$$

Now, the diagonal elements in Eq. (2) are bigger than the off-diagonal elements in magnitude since $\cos(\pi/8) > \sin(\pi/8)$, so that the RZ model is less mixing of the two representations than the LZS model. It naturally pushes Eq. (2) into,

$$\tan(2\theta(R_0)) = 0 \Rightarrow \theta(R_0) = 0, \tag{15}$$

which leads Eq. (2) to be unity matrix, there is no mixing case and thus there is no nonadiabatic transition at all. From analysis discussed above, we can conclude that any unified semiclassical theory must include this diabatic-to-adiabatic transformation angle that is actually representing a type of nonadiabatic transition.

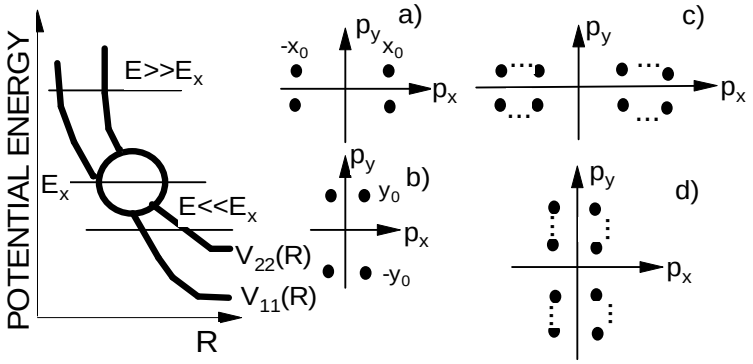

Figure 1. General two-state potential energy surface diagram; $E > E_X$ corresponds nonadiabatic transition zone and $E < E_X$ corresponds to nonadiabatic tunneling zone. The circled area determines the important parameter d in Eq. (16). Distribution of four transition points in complex momentum plane for the LZS model: (a) $E >> E_X$ and (b) $E << E_X$. Distribution of infinite transition points in complex momentum plane for the Nikitin model: (c) $E >> E_X$ and (d) $E << E_X$.

We can use the following parameter to determine a type of nonadiabatic transition,

$$d \equiv d(R_0) = 1 + \frac{4V_{12}^2(R_0)}{[V_{22}(R_0) - V_{11}(R_0)]^2}. \tag{16}$$

Unified semiclassical theory now means that the Stokes constant U_1 must be function of the parameter d in Eq. (16). The other two parameters that the Stokes constant should contain are σ and δ defined by

$$\sigma + i\delta = \int_{T_1}^{R^*} p_1(R)dR - \int_{T_2}^{R^*} p_2(R)dR \tag{17}$$

where $p_1(R)$ and $p_2(R)$ are defined in Eq. (8), and the complex crossing point R^* is given in Eq. (12).

Calculations

We illustrate some numerical examples and compare calculations between exact quantum mechanics and the present unified analytical semiclassical theory for overall nonadiabatic transition probability defined from the reduced scattering matrix in Eq. (10),

$$P_{12} = |U_2|^2 = \left| \frac{U_1 - U_1^*}{1 + U_1^* U_1} \right|^2, \tag{18}$$

in which the Stokes constant U_1 is given in the case $E > E_X$ for nonadiabatic transition, and by Eq. (18) in the case $E < E_X$ for nonadiabatic tunneling. Three parameters d, σ and δ are calculated from Eq. (16) and (17), respectively. Exact calculations are performed from a quantal close-coupling method.

a. Nonadiabatic transition case E > E_X

The first example is crossing model potentials from the He^+ + Ne system and its functional forms in diabatic representation. The most important parameter in Eq. (16) is calculated as d = 7.3 that is far from the LZS case where $d = \infty$. Figure 3a shows very good agreement between exact results and unified analytical semiclassical calculations, and both the LZ and the RZ formulas give relatively good results in a lower energy range and gradually become bad as collision energy increases. The second example is noncrossing model modified from the first example and its functional forms in diabatic representation. The most important parameter in Eq. (16) is designed as d = 2 that is exactly the RZ case. Figure 3b shows very good agreement between exact results and unified analytical semiclassical calculations, while both the LZ and the RZ formulas give bad results, and the RZ formula seems presenting correct oscillating structure.

b. Nonadiabatic tunneling case E <E_X

The third example is general experiential model. The most important parameter in Eq. (16) is calculated as d = 2.28. Figure 4a shows very good agreement between exact results and unified analytical semiclassical calculations, while the ZN formula (Eq. (18) with $d = \infty$) does not work well. The fourth example is modified from the third example by letting the most important parameter in Eq. (16) be d = 1.2 so that nonadiabatic tunneling probability should be very small. Figure 4b shows very good agreement between exact results and unified analytical semiclassical calculations, while the ZN formula becomes very bad.

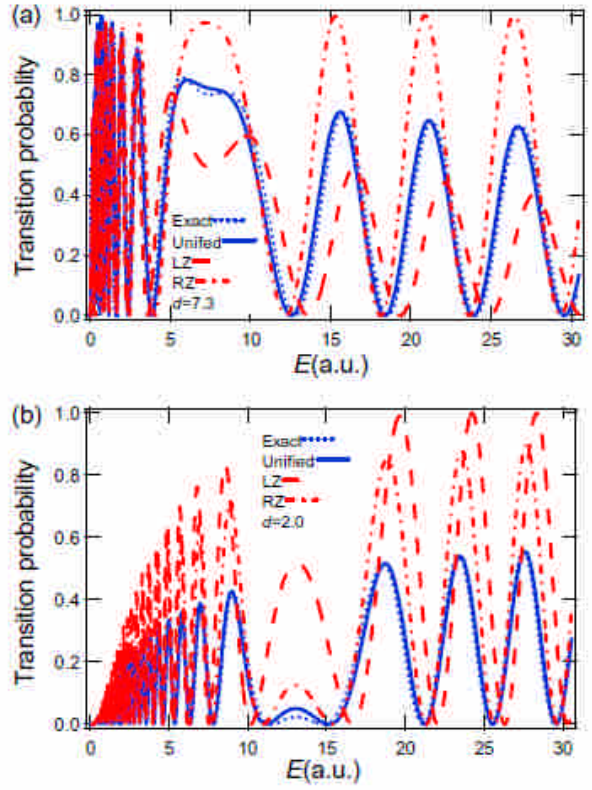

Figure 3. Overall non-adiabatic transition probability P_{12} as a function of the total energy E. Dotted lines are the results of the quantum mechanical close-coupling method, solid lines are the results from the unified analytical semiclassical formula, dashed lines are the results of the LZ formula, and dash-dotted lines are the results of the RZ formula. (a) $d = 7.3$ and (b) $d = 2.0$.

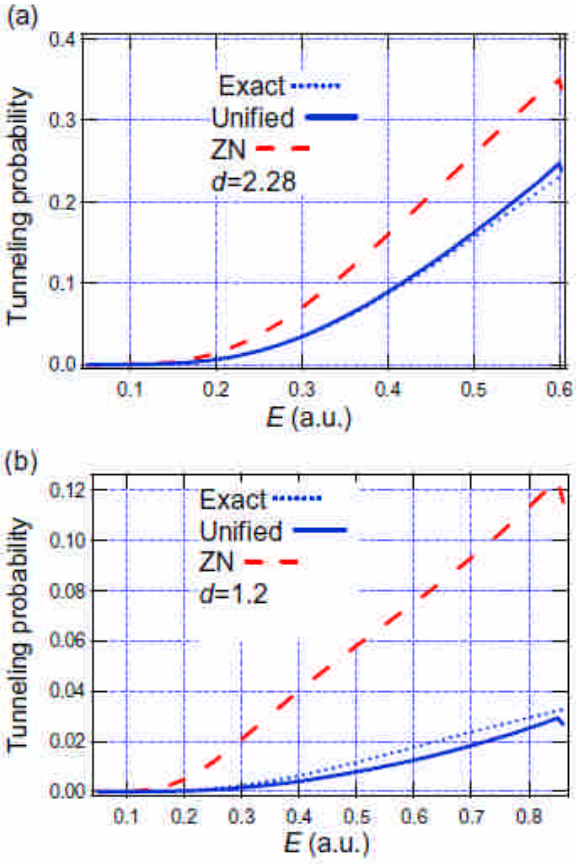

Figure 4. Overall non-adiabatic tunneling probability P_{12} as a function of the total energy E. Dotted lines are the results of the quantum mechanical close-coupling method, solid lines are the results of the unified analytical semiclassical formula, and dashed lines are the results of the ZN formula. (a) $d = 2.28$ and (b) $d = 1.2$.

Concluding remarks

Unified analytical semiclassical theory for general two-state nonadiabatic transition is reviewed within the WKB framework associated with the Stokes phenomenon in mathematics. The reduced scattering matrix is expressed in terms of a single complex quantity that is called Stokes constant U_1. Distributions of transition points that are complex crossing points between two adiabatic potential energy surfaces show certain symmetry and separable pattern in certain limiting cases (see Fig. 1). This is essential for the WKB method to derive a compact analytical expression for U_1. Since U_1 is function of three parameters; the most important one is in Eq. (16) that represents type of nonadiabatic transition and the other two in Eq. (17) represent effective magnitude and phase of nonadiabatic transition.

There are two ways to apply unified analytical semiclassical theory for multidimensional nonadiabatic dynamics. The first way is to separate multidimensional coordinates into internal coordinates and reaction coordinate that is curved one dimension. In this way, one converts problem into one-dimensional many-state nonadiabatic transitions, and then so called two-by-two state method can come to apply. The second way is to directly incorporate with trajectory surface hoping method and compute hoping probability analytically along trajectory. Analytical formula here can also be easily applied to various boundary conditions for multidimensional wave function and trajectory.

9. “Ab initio studies of excited electronic state S2 of pyrazine and Franck-Condon simulation of its absorption spectrum,”
R. X. He, **C. Zhu***, C. H. Chin, S. H. Lin,
Published on Chem. Phys. Lett. 476, 19(2009)

Abstract

Equilibrium geometry and its 24 vibrational-normal-mode frequencies of the excited state $S_2(^1B_{2u})$ of pyrazine are calculated and characterized using the complete active space self-consistent field method in the adiabatic representation. The displaced harmonic oscillator approximation is used to simulate the absorption spectrum of the $S_2(^1B_{2u})$ state along with the Franck-Condon approximation. It is found that the totally symmetric mode ν_1 plays the most important role and this exactly agrees with the experimental observations. The simulated absorption spectrum agrees well with those experimentally observed. This indicates that the present $S_2(^1B_{2u})$ state calculated in the adiabatic representation effectively includes contribution from the diabatic vibronic coupling through the conical intersection.

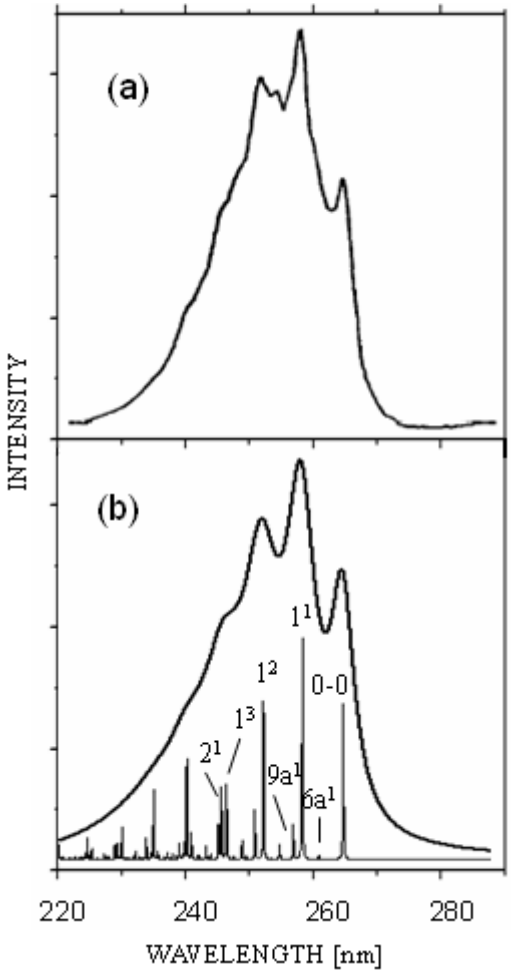

Fig. 2. $S_2(^1B_{2u})\leftarrow S_0(^1A_g)$ absorption spectrum of pyrazine. (a) Experimental data and (b) spectrum from the present calculations. The stick spectrum is simulated by taking a phenomenological dephasing time of about 20 fs.

Publications supported by NSC-97-2113-M-009-010-MY3

1. L.Yang, **C. Zhu***, J. G.. Yu, and S. H. Lin, "Anharmonic Franck-Condon simulation of the absorption and fluorescence spectra for the low-lying S1 and S2 excited states of pyrimidine," Chem. Phys. (in press, 2012). (NSC-97-2113-M-009-010-MY3)(IP:2.06)

2. Q. Yang, R. He*,W. Shen, H. Li, M. Li, **C. Zhu*** and S. H. Lin "Excited State ab Initio and Franck Condon Simulation of S1 f S0 Fluorescence Excitation Spectra of p-, m-, and o-Difluorobenzenes," J. Phys. Chem. A, 115, 14022 (2011). (NSC-97-2113-M-009-010-MY3)(IP:2.732)

3. C.-K. Lin*, Y. Niu, **C. Zhu**, Z. Shuai, and S. H. Lin, "The Role of the np* 1Au State in the Photoabsorption and Relaxation of Pyrazine," Chem. Asian J., 6, 2977 (2011). (NSC-97-2113-M-009-010-MY3) (IP:4.188)

4. R. He, L. Yang, **C. Zhu***, M. Yamaki, Y-P. Lee, and S. H. Lin, "Franck-Condon simulation of the A 1B2→X 1A1 dispersed fluorescence spectrum of fluorobenzene and its rate of the internal conversion," J. Chem. Phys. 134, 094313 (2011) (NSC-97-2113-M-009-010-MY3) (IP:2.928)

5. L. Zhang, C. R. Zhu, G. Jiang, **C. Zhu*** , and Z. H. Zhu, "A quasiclassical trajectory study of reactive scattering on an analytical potential energy surface for GeH2 system," Journal of Theoretical and Computational Chemistry 10, 147(2011). (NSC-97-2113-M-009-010-MY3) (IP:0.8)

6. J. Li, C-K. Lin*,X. Y. Li, **C. Zhu** and S. H. Lin, "Symmetry forbidden vibronic spectra and internal conversion in benzene," Phys.Chem.Chem.Phys.12, (2010), pp14967-14976(NSC-97-2113-M-009-010-MY3) (IP:3.454)

7. H. Wang, **C. Zhu***, J. G. Yu, and S. H. Lin, "Anharmonic Franck–Condon simulation of the absorption and fluorescence spectra for the low-lying S1 and S2 excited states of pyridine," J. Phys. Chem. A, 2009, 113 (52), pp 14407–14414 (NSC-97-2113-M-009-010-MY3) (IP:2.871)

8. **C. Zhu*,** "Analytical semilcassical theory for general nonadiabatic transition and tunneling," Phys. Scr. 80, 048114 (2009). (NSC-97-2113-M-009-010-MY3) (IP:0.970)

9. R. X. He, **C. Zhu***, C. H. Chin, S. H. Lin, "Ab initio studies of excited electronic state S2 of pyrazine and Franck-Condon simulation of its absorption spectrum," Chem. Phys. Lett. 476, 19(2009). (NSC-97-2113-M-009-010-MY3)(IP:2.169)